Matrix Biology Plus 24 (2024) 100161

Contents lists available at ScienceDirect

Matrix Biology Plus

journal homepage: www.sciencedirect.com/journal/matrix-biology-plus

Profiling of collagen and extracellular matrix deposition from cell culture using in vitro ExtraCellular matrix mass spectrometry imaging (ivECM-MSI)

Stephen C. Zambrzycki [a], Samaneh Saberi [b], Rachel Biggs [c,d], Najmeh Eskandari [a], Davide Delisi [a], Harrison Taylor [a], Anand S. Mehta [a,b], Richard R. Drake [a,b], Saverio Gentile [a,b], Amy D. Bradshaw [c,d], Michael Ostrowski [b,e], Peggi M. Angel [a,b,*]

[a] Department of Cell and Molecular Pharmacology, MUSC, Charleston, SC, USA
[b] Hollings Cancer Center, Charleston, SC, USA
[c] Department of Medicine, MUSC, Charleston, SC, USA
[d] The Ralph H. Johnson Department of Veteran's Affairs Medical Center, Charleston, SC, USA
[e] Department of Biochemistry and Molecular Biology, MUSC, Charleston, SC, USA

ARTICLE INFO

Keywords:
Extracellular matrix
Collagen proteomics
Collagen proline hydroxylation
Cell culture
Rapid profiling
Mass spectrometry imaging

ABSTRACT

While numerous approaches have been reported towards understanding single cell regulation, there is limited understanding of single cell production of extracellular matrix phenotypes. Collagens are major proteins of the extracellular microenvironment extensively used in basic cell culture, tissue engineering, and biomedical applications. However, identifying compositional regulation of collagen remains challenging. Here, we report the development of In vitro ExtraCellular Matrix Mass Spectrometry Imaging (ivECM-MSI) as a tool to rapidly and simultaneously define collagen subtypes from coatings and basic cell culture applications. The tool uses the mass spectrometry imaging platform with reference libraries to produce visual and numerical data types. The method is highly integrated with basic in vitro strategies as it may be used with conventional cell chambers on minimal numbers of cells and with minimal changes to biological experiments. Applications tested include semi-quantitation of collagen composition in culture coatings, time course collagen deposition, deposition altered by gene knockout, and changes induced by drug treatment. This approach provides new access to proteomic information on how cell types respond to and change the extracellular microenvironment and provides a holistic understanding of both the cell and extracellular response.

Introduction

Increasingly, contemporary literature defines that the extracellular microenvironment has a significant impact on cell phenotype in health and disease [1–3]. Collagens are a major component of the extracellular matrix (ECM) and play a significant role in localized cellular microenvironments primarily through compositional changes and superstructural regulation by post-translational modification [4–6]. These factors work to influence cell signaling, tissue stiffness, therapeutic success, disease progression, and patient outcomes [7–11]. The creation of collagen-based ECM biomaterials for improved cell targeting is a focus for biomedical applications, control of cell culture, and tissue engineering [12–18]. However, the collagens expressed by cells in culture or used in research and drug development are poorly characterized if characterized at all. This is due to a lack of tools available that can sensitively assess collagen structure and composition.

Approaches for evaluation of collagen composition and translational regulation of specific collagen types are primarily qualitative. Second harmonic generation microscopy, super resolution microscopy, and atomic force microscopy measure physical changes to collagen in cell culture, but very little information is extracted about specific chemical translational and post-translational modifications [19–23]. Immunofluorescence staining provides remarkable sensitivity for collagen detection and defining collagen types with low numbers of cells;

Abbreviations: ECM, extracellular matrix; HYP, hydroxyproline; ivECM-MSI, In vitro ExtraCellular Matrix Mass Spectrometry Imaging; LC-MS/MS, liquid chromatography tandem mass spectrometry; LVAD, left ventricular assist device; MALDI, matrix-assisted laser desorption ionization; MSI, mass spectrometry imaging; PCAF, pancreatic cancer associated fibroblast; PTM, post-translational modification.

* Corresponding author at: 173 Ashley Ave, BSB358, Charleston, SC 29425, USA.
E-mail address: angelp@musc.edu (P.M. Angel).

https://doi.org/10.1016/j.mbplus.2024.100161
Received 11 March 2024; Received in revised form 19 September 2024; Accepted 19 September 2024
Available online 25 September 2024

however, they lack information about specific chemical translational and post-translational modifications as well [24,25]. In vitro analysis on ECM expressed by cell culture are limited and require large numbers of cells to produce sufficient ECM to characterize by conventional proteomic methods. The majority of proteomic approaches use liquid chromatography tandem mass spectrometry (LC-MS/MS) to measure collagen deposition in vitro, including post translational modifications [26–33]. These experiments can be time consuming, lack spatial information about the distribution of collagen types in cell culture, and require specialized enrichment procedures prior to analysis. Extracellular visualization by secondary ion mass spectrometry has demonstrated the ability to detect amino acid changes associated with collagen regulation in cytokine challenged matrices [34]. There is continued need for approaches that can report compositional changes from the minimal cell numbers used in basic biology or bioengineering experiments.

We have adopted previously published approaches for collagen targeted tissue imaging on fresh frozen and formalin-fixed, paraffin embedded samples [35,36]. This methodology scans tissue by matrix-assisted laser desorption ionization (MALDI) mass spectrometry imaging to define collagen composition in ex-vivo, biopsy, and resected tissue sections. The current study reports In vitro ExtraCellular Matrix Mass Spectrometry Imaging (ivECM-MSI). This approach adapts the MALDI mass spectrometry imaging platform with reference libraries as a scanning proteomics tool to define the spatial distribution of ECM composition in coatings and in cultured cells. The developed workflow is demonstrated in four different applications in this study spanning different cell types and scenarios in cultured cells, including measurement of collagen surface coating, time courses, gene silencing, and drug treatment. This work provides a significant advancement towards holistic evaluation of collagen protein composition in biomedical and bioengineering research.

Results

Approach overview

The goal of the current study was to develop approaches that can report on the extracellular matrix composition secreted by low numbers of cells used in biomedical and bioengineering research studies. The approach, termed In vitro ExtraCellular Matrix Mass Spectrometry Imaging (ivECM-MSI) (Fig. 1), allows assessment of collagen protein composition from as few as 2,500 cells per well. The approach was purposefully developed to be highly integrative with conventional biological experiments. As such, the method uses common glass slides with wells for cell culture, followed by decellularization using basic pH washes. After rinsing and drying, a mixture of proteases that target the extracellular matrix is applied to the slide and incubated for digestion. A chemical matrix is applied to the slide to facilitate rapid scanning by MALDI coupled with high mass resolution, high mass accuracy instrumentation. Similar to the MALDI Biotyper [37,38], rapid scanning is coupled with reference libraries that are curated lists of sequenced peptides derived from same-sample sources such as cells, tissues or coating solution. The scanning approach using the mass spectrometry imaging platform coupled with reference libraries allows multiple types of experiments on ECM from minimal numbers of cells such as time

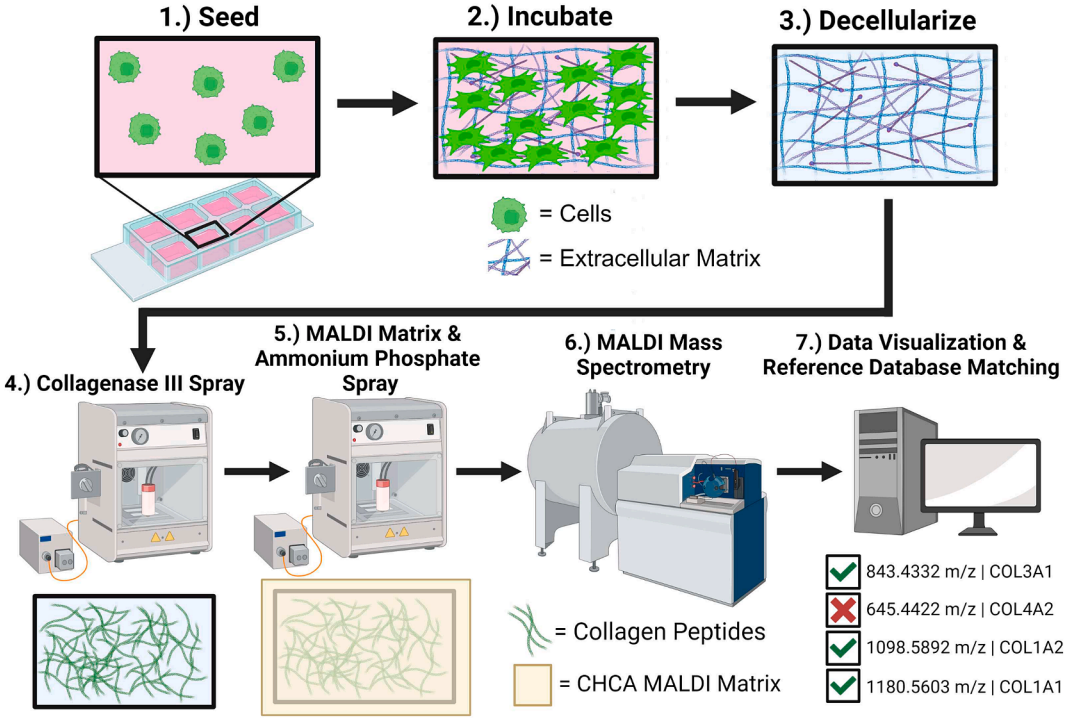

Fig. 1. Workflow for in Vitro ExtraCellular Matrix Mass Spectrometry Imaging (ivECM-MSI). 1.) Cells are seeded on Nunc Lab-Tek II glass chamber slides. Gelatin can be used as a coating prior to seeding if certain cell lines are not adhering to the glass. 2.) Cells are incubated in the glass chambers slides until confluence. 3.) The medium is removed and each well in the chamber slide is then decellularized with a 20 mM ammonium hydroxide solution for 5 min. Each well is then rinsed 4 times with sterile water. Next, the chambers are removed from the slide. Afterword, the slide is dried in a vacuum desiccator. Slides can be stored in a −20 °C freezer for temporary storage if needed. 4.) A 0.1 mg/mL solution of collagenase III is sprayed evenly onto the slides. The collagenase sprayed slides are then incubated in a 37 °C humidity chamber for 5 h to digest the collagen into peptides. Afterword, the slides are dried in a vacuum desiccator. Slides can be stored in a −20 °C freezer for temporary storage if needed. 5.) The collagenase digested slides are then sprayed evenly with a 7 mg/mL α-cyano-4-hydroxycinnamic acid (CHCA) solution. Immediately after CHCA spraying, a 5 mM ammonium phosphate solution is sprayed on top of the MALDI matrix to minimize matrix cluster formation. Slides at this stage can be temporarily stored in a vacuum desiccator if needed. 6.) The matrix sprayed slides are loaded into the MALDI mass spectrometer for MALDI mass spectrometry analysis. 7.) Finally, the data is visualized through mass spectrometry imaging heatmaps, *m/z* features are searched through a collagen peptide database, and statistics are performed. Created with BioRender.com.

course, drug dosing and genetic variation. The spatial aspect may be further leveraged against migration assays, co-culture, differentiation, and drug diffusion work. We envision using rapid scanning experiments to identify ECM variations as targets of the biology. This can be followed by the standard approach growing of millions of cells for comprehensive systems biology at a specific point, e.g., time, drug dose. The starting points for building the rapid scanning and reference libraries are common biomedical and bioengineering experiments, evaluating collagen surface coatings and monitoring time courses of deposition. The ivECM-MSI approach shows the ability to distinguish ECM secreted by genetically modified fibroblasts and cells that were drug treated.

Quantitative measurement of collagen as a surface coating

Surface coatings play a critical role in cell signaling, migration and differentiation, used in implant biology and cell growth [39–41]. The protein composition of most surface coatings are largely undefined, leading to batch effects and inconsistencies in cell culture. To evaluate ivECM-MSI as an approach to reporting on surface coating composition, a titration of rat tail collagen coatings was measured from 0 μg/cm^2 to 160 μg/cm^2 on four separate slides following the manufacturers protocols for coating wells (Fig. 2). Significantly, the approach allows data visualization of coating distribution which can be leveraged for quality control in biomanufacturing to understand the role of uneven coatings on cellular genomic, proteomic, and metabolomic homogeneity (Fig. 2A). In this example, although coating was applied uniformly through careful protocols, the actual distribution in each well reflects some left-to-right differences in distribution. Spectral detection directly from the surface of each well shows highly multiplexed feature detection (Fig. 2B). Differential feature detection at 16X the concentration of conventional surface coating concentrations for cell culture may be due to diffusive processes associated with more concentrated coatings. Reference libraries provide curated same-sample peptide collections to match to rapid scanning approaches, including compositional and post-translational modification differences (Fig. 2C, Supplemental Fig. S1). Reference libraries are constructed by same-sample collagenase digestion and curated into peak lists that allow matching of the high throughput collected data to collagen peptides including post-

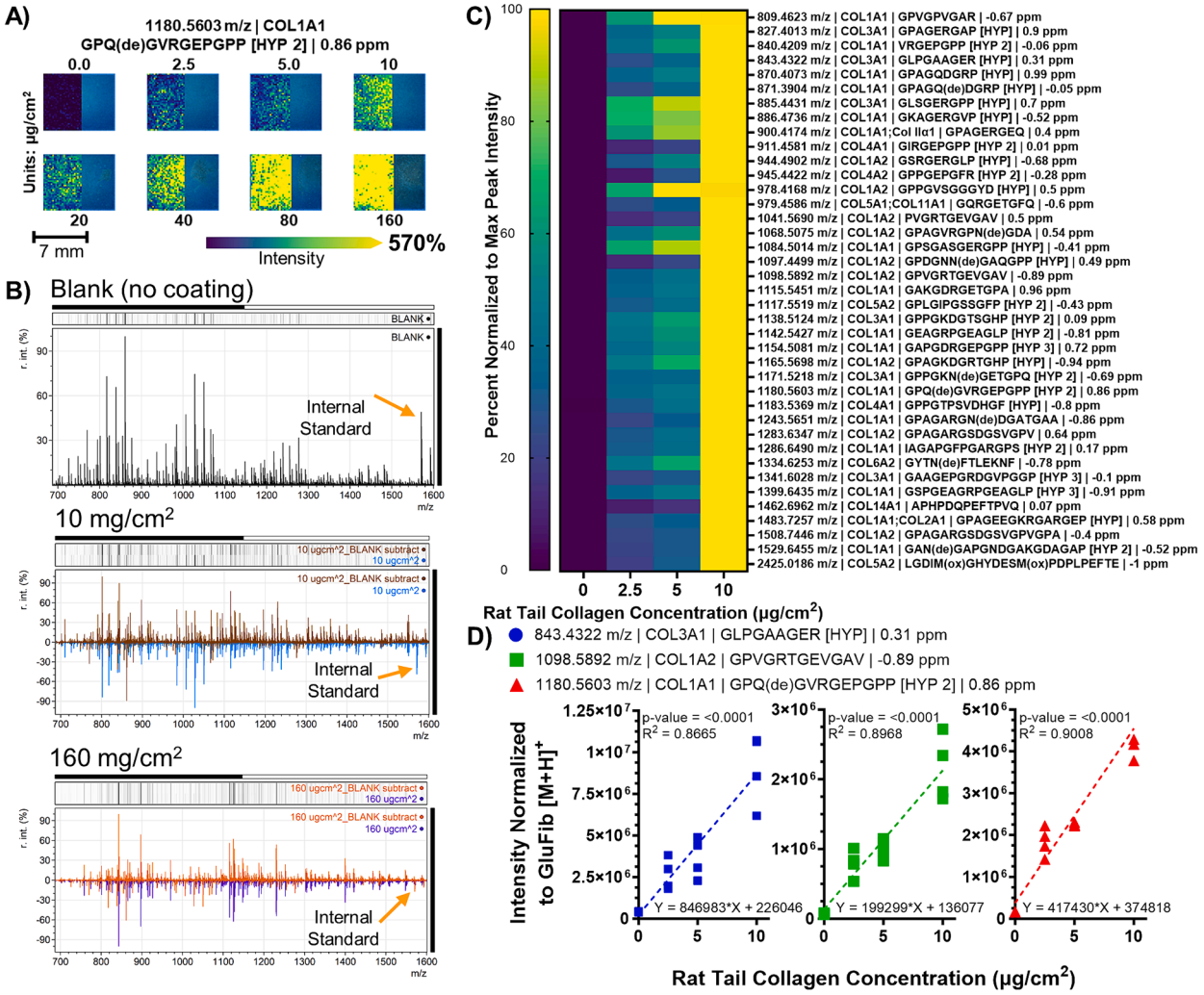

Fig. 2. Evaluating the performance of ivECM-MSI using rat tail type I collagen coatings on 4 separate slides and development of a reference database. A) Example surface coating visualization to detect differential surface coating distribution. The image is a heatmap of the feature 1180.5593 *m/z*, collagen α1(I) (GPQ(de)GVRGEPGPP [HYP 2]). B) Spectral feature detection by slide scanning using mass spectrometry imaging. Example spectra from typical surface coating concentrations used in cell surface coating (10 mg/cm^2) compared to highly concentrated amounts (160 mg/cm^2) are shown. The internal standard is (Glu1)-Fibrinopeptide B human used to normalize signal intensities between experiments. C) Reference library matching image data. Reference library reports detection of differences in collagen composition and in variable post-translational modifications. D) Example quantification for typical concentrations tested for cell culture coatings with conventional coating protocols. Each data point is a measurement from one of the slides, n = 4 technical replicates (n = slide). [HYP] = 1x hydroxylated proline site; (de) = deamidation of asparagine or glutamine; (ox) = methionine oxidation; ppm- parts per million match by mass accuracy.

translational modification and compositional changes. This strategy is analogous to the MALDI BioTyper strategies (reviewed in [37]) that use bacterial signatures by high throughput scanning to identify microorganisms in clinical microbiology. For coating, the majority of collagen detected was collagen alpha-1(I) chain (COL1A1), composition included Collagen alpha-2(I) chain (COL1A2), collagen alpha-1(IV) chain (COL4A1), and collagen alpha-1(XIV) chain (COL14A1). Biology specific collagen triple helical formation involves variation in hydroxylation of proline (HYP) that contributes to cell binding with subsequent downstream signaling effects [42]. The ivECM-MSI approach demonstrated detection of post-translational modifications. Importantly, not all prolines in each were modified, thus representing new information that can be used in refining experiments and understanding how coating composition may contribute to cellular expression. Not all peptides showed a linear response (Fig. 2D, Supplemental Fig. S2, Supplemental Table S1) supporting that at certain coating levels

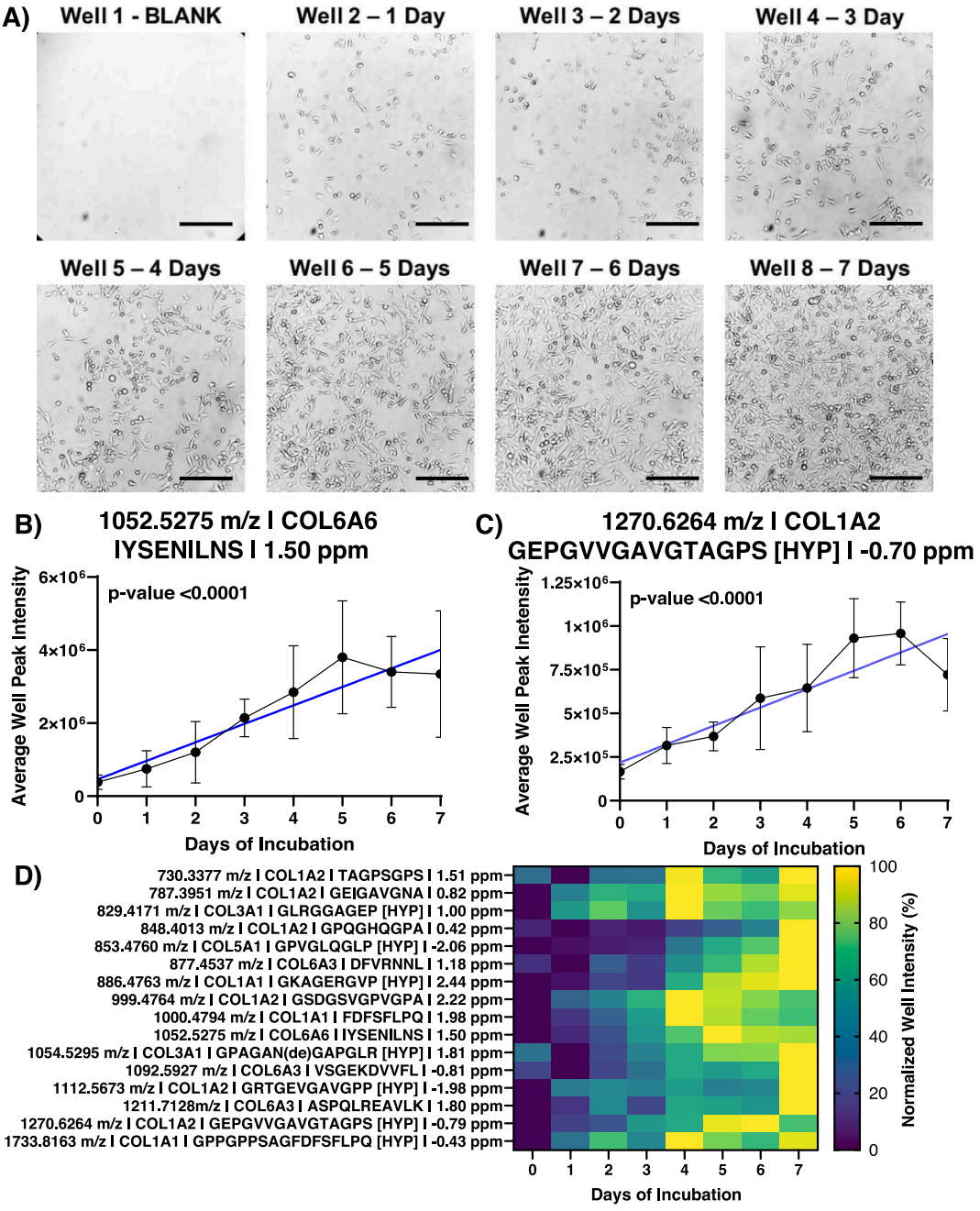

Fig. 3. Monitoring the deposition of various oncogenic collagen peptides in MDA-MB-231 triple negative breast cancer (TNBC) cells over 7 days using ivECM-MSI on four separate slides and our tissue reference database. A) 10x brightfield microscope images monitoring the confluence of each well over the 7-day period. Response curves for the incubation titration experiment monitoring oncogenic collagen type putative $[M+H]^+$ peptide feature deposited over 7 days for B) collagen α6(VI) and C) collagen α2(I). Day 0 on the scatter plots is the blank well 1. The center of each data point is the mean and error bars equate to the standard deviation, n = 4 technical replicates (n = slide). D) Normalized heatmap of the 7-day deposition of MDA-MB-231, from 4 technical replicates (n = slide) for 16 $[M+H]^+$ collagen peptide features detected. All the features are putatively identified within 2.5 ppm mass accuracy. Each feature label includes detected *m/z*, putative protein ID, putative peptide sequence with post translational modifications, and parts per million mass deviation from the theoretical $[M+H]^+$ value. [HYP] = 1x hydroxylated proline site; (de) = deamidation of asparagine or glutamine; (ox) = methionine oxidation; ppm- parts per million match by mass accuracy.

there may be differential diffusion of certain collagen types due to a selective affinity from the culture surface and collagen solution. Here, the collagen coating concentrations ranged from 0 μg/cm^2 to 10 μg/cm^2 which are typical coating concentrations for cell culture conditions. Further analysis showed reported high multiplexing with the identification and quantification of up to 79 features derived from surface coating composition (Supplemental Fig. S2, S3, & S4; Supplemental Table S2 & S3). Overall, the approach demonstrated the ability to visually detect distribution of relevant amounts of collagen applied as surface coating and detail critical protein composition contributing to cellular response.

Collagen deposition time course study over 7 days

Time-course monitoring is used to evaluate effects such as cell quality, differentiation patterns, and drug treatment [43–45]. To test the approach for time course monitoring, collagen deposition from triple negative breast cancer cells MDA-MB-231 was characterized over a 7-day period with 10,000 cells seeded per well on four separate slides (Fig. 3). Detection of collagen deposition occurred over a variety of confluence points throughout the 7-day time course as shown in the brightfield images (Fig. 3A). The response curve of a putative peptide feature from the tissue reference database for beaded filament forming collagen α6(VI) is shown in Fig. 3B. The collagen α6(VI) peptide shows an increasing peak intensity up to day 5, with the signal plateauing at days 6 & 7. Lower COL6A6 gene expression has been associated with a later pathological stage and larger tumor size in breast cancer, thus supporting higher detection during the time course [46].

A plateauing effect was seen in a putative peptide feature of fibril forming collagen α2(I) (Fig. 3C). The response curve shows an increasing deposition of the putative peptide for collagen α2(I) (Fig. 3C) up to day 6, with the intensity of the putative peptide signal plateauing off at day 7. Increased COL1A2 gene expression has been linked to worse prognosis in many cancers [47–49]. A heatmap of 16 putatively identified collagen peptide features from the tissue reference database show that collagen composition changes during the time course, likely in response to decreasing distance to nearby cells (Fig. 3D, Supplemental Fig. S5-8). Interestingly, the approach was able to detect cell-secreted collagen domains modified by hydroxylated proline, useful for understanding modulation of cell binding domains. Reference database building for MDA-MB-231 further detected 6 features not found in published tissue databases (Supplemental Fig. S9 & S10). Further, other extracellular matrix proteins and cell culture media components were also detected (Supplemental Tables S4 and S5). In summary, the approach allowed detection, time course monitoring, and relative quantification of changes in collagen composition from minimal numbers of a single cell type.

Collagen deposition modulated by drug treatment

Many drug therapies have been developed to regulate collagen deposition in a variety of diseases such as pancreatic cancer, non-alcoholic steatohepatitis, idiopathic pulmonary fibrosis, and colorectal cancer [50–53]. The developed approach was tested for monitoring collagen deposition changes during activation of the cellular senescence program in human-derived lung cancer cells by stimulation of the Kv11.1 potassium channel with the selective activator molecule NS1643 in three separate wells (Fig. 4) [54–56]. A senescent-like phenotype was achieved after 24 h treatment with NS1643 compared with untreated cells (Fig. 4A–B) as demonstrated by an arrest of the cell cycle in G0/G1 and upregulation of the senescent marker and tumor suppressor p21$^{cif1/waf1}$ after treatment (Fig. 4C). Treated cells stains positive for SA-β-gal, a marker associated with senescence (Fig. 4D). After treatment, ivECM-MS was completed on the same wells, following protocols for decellularization and scanning. An example of increased deposition of the putative peptide features for fibrillar collagen α1(I) (Fig. 4E) and fibril-associated collagen α1(XIV) (Fig. 4F, Supplemental S11). Importantly, this also demonstrates capabilities in capturing cell signaling information by immunostaining from the same wells for simultaneous investigations of both cellular and extracellular biology. The data shows that along with phenotypic changes induced by drug treatment the deposition of collagen composition is altered.

Collagen deposition influenced by high blood pressure medication spironolactone treatment of primary cardiac fibroblasts from left ventricular assisted device patients was used as a further case study testing stability in storage when evaluating drug treated samples. Here, drug treatment altered fibroblast output; evaluation of the same sample after three-day vacuum storage demonstrated no difference in signal intensity detected by the approach (Supplemental Fig. S12). In total, the approach was able to detect compositional changes due to drug treatment from as few as 2500 cells shown in both primary cell types derived from patients.

Collagen deposition by models of genetic deletion

Gene knockout studies can provide valuable insight into the construction of the extracellular matrix network through differential protein expression. Previous work has demonstrated that loss of PTEN expression in cancer changed collagen fiber measurements and is associated with poor outcomes [57]. Collagen deposition by fibroblasts from a STAT3 knockout mouse (n = 2) and its wild type parent (WT1; n = 2), and fibroblasts from a PTEN knockout mouse (n = 4) and its wild type parent (WT2; n = 4) were compared to one another (Fig. 5). After 3 days of expansion, morphological changes were observed (Fig. 5A). Immunofluorescent staining of the PCAF cells demonstrated uniform secretion of vimentin, an intermediate filament marker for cells of mesenchymal origin, including fibroblasts [58] (Fig. 5B). STAT3 and PTEN proteins expression were observed in all wild type cells, indicating a predominantly cytoplasmic localization for STAT3 protein and a nuclear localization for PTEN protein. The Western blot analysis further confirmed gene deletion of STAT3 and PTEN expression (Fig. 5C).

Type 1 collagen plays numerous roles in pancreatic cancer and deletion of the collagen α-1(I) gene in myofibroblasts can accelerate disease progression [59,60]. Here, the PTEN knockout fibroblasts demonstrated increased deposition of the putative peptide feature for collagen α1(I) (GPIGNVGAP; unmodified) (Fig. 5D). Examples of 50 collagen peptides secreted by the fibroblasts with reference to the tissue database shows differential deposition by the genetically modified cell types, 11 additional collagen and other extracellular matrix protein & media features not found in the published tissue databases (Fig. 5E, Supplemental Table S6 S5 & S7, Supplemental Fig. S13 & S14, Supplemental Fig. S15 & S16). The bovine gelatin coating surface used for adherence did not contribute significantly to the background. The approach performed on mouse fibroblasts demonstrates that using an enzyme such as bacterially derived collagenase in the workflow produces activity unbiased to species and thus differentiates coating derived from another species. In total, ivECM-MSI detected significant compositional changes due to genetic manipulation, unbiased to species without changes to the basic biological experimental strategies, e.g., no special growth conditions or surfaces for mass spectrometry scanning. The approach thus allows for a controlled method to understand the changes to the extracellular proteome produced by altering gene expression in any species.

Discussion

In this work, we present a new analytical approach, In vitro Extra-Cellular Matrix Mass Spectrometry Imaging (ivECM-MSI) designed to report on proteomic composition of the extracellular microenvironment produced by cells in culture. Enzyme-specific targeting of collagen protein composition is accessed through the use of collagenase type III, which by tissue imaging mass spectrometry specifically reports on collagen types and 40–60 other extracellular proteins [36,61–64].

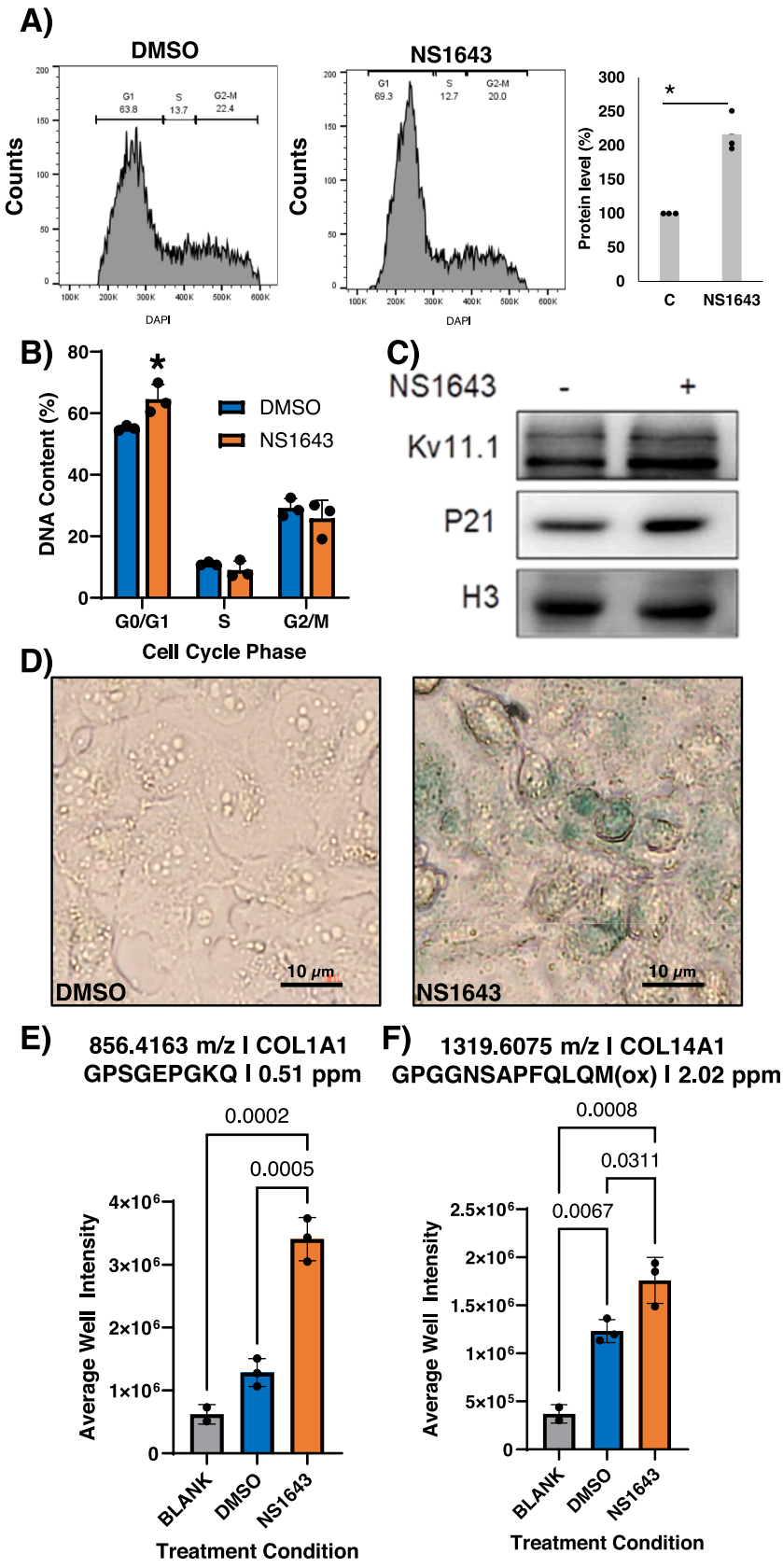

(caption on next page)

Fig. 4. Deposition of collagen in H1299 lung carcinoma cells treated with DMSO and NS1643 Kv11.1 potassium channel activator. A) Identification and quantification of cellular senescence by flow cytometry of representative DNA content in H1299 cells before and after NS1643 treatment (50 μM for 24 h). Protein level is p21 in control (C) vs NS1643 treated cells. B) Percent change of cell accumulation for G0/G1, S and G2/M phases of the cell cycle (n = 3 technical replicates (n = well); *=$p < 0.05$). C) Example western blots showing the expression level of Kv11.1 and senescent marker $p21^{cip1/waf1}$ in H1299 cells treated with DMSO and NS1643 (50 μM/24 h; n = 3; *=$p < 0.05$). No change of Kv11.1 protein was observed after treatment (control). D) Senescence-associated β-galactosidase (SA-β-gal) staining. Representative images of H1299 cells treated with (DMSO, left) or NS1643 (50uM/24hr, right) as indicated. Cells were treated with the Kv11.1 activator NS1643 (50 μM/48 hr) to induce cellular senescence. Histogram of average well peak intensities for the putative $[M+H]^+$ peptide for E) fibril forming collagen α1(I) and F) fibril-associated collagen α1(XIV) for both slides seeded at 2E5 cells. The center of each data point is the mean and error bars equate to the standard deviation. After one-way ANOVA analysis and Tukey multiple comparisons test, only significant Tukey p-values ≤ 0.05 are displayed. (ox) = methionine oxidation; ppm- parts per million match by mass accuracy. ivECM-MSI measurements were on two four chamber well slides three separate wells.

Collagenase III binds to the collagen structure with a strong protease specificity towards G-P-X or G-X-P regions, where P can be unmodified or modified proline [65,66]. An advantage of using enzymes, not antibodies to access the extracellular proteome is multifold. There are few antibodies that have epitope recognition to the complexities of the collagen structure, to include post-translational modifications. Antibody-based assays are species specific and few antibodies exist for reporting the complete complexities of collagen types within a single experiment. The concept of enzyme specific targeting for proteomic building and mass spectrometry imaging further allows significant multiplexing with other enzymes, imaging, and molecular modalities [67–70]. This approach also produces a tiered system for study purposes. Rapid scanning by mass spectrometry imaging may be used to evaluate for changes in extracellular response to treatments. The use of the mass spectrometry imaging platform produces output data that may be read as both visual output for quality control and/or numerical data, useful in multiple types of advanced data modeling. Peptide *m/z* reference libraries generated from previous LC-MS/MS studies built using an independent workflow represents a significant amount of initial work but can be leveraged downstream for high throughput screening and fingerprinting. This study leveraged previous publications reporting collagen structure as well as building peptide *m/z* reference libraries specific to each experiment. For cell culture studies, reference libraries were built from very small cell numbers (2,000–10,000) at specific time points. This was done to capture profiles from relevant cell numbers at very specific timepoints. It is possible to build comprehensive databases from larger cell numbers that can then be used as a reference library in monitoring experimental conditions. However, it is known that extracellular composition changes with numbers of cells and over time [71]; thus larger cell numbers may yield different composition. A combination of a large and small cell number database may be necessary for comprehensive sequence coverage of the collagen and better highlight heterogeneity between experiments, respectively. The developed proteomic approach leveraged ion mobility for sensitive reference library building. Ion mobility is used as a parallel separation technique with mass spectrometry that leverages molecular surface area to separate isomers from one another. Ion mobility produces information which may be used to distinguish sites of collagen hydroxylated proline variation. Development of collision cross sections for use in monitoring extracellular composition by mass spectrometry imaging uses systematic synthesis and collision cross section measurement of hydroxylated proline variants [36]. The overall findings demonstrate that ivECM-MSI is a tool that facilitates investigations of extracellular matrix composition secreted by single cell types at the translational and post-translational level.

ivECM-MSI was tested over a variety of applications relevant to understanding composition of the extracellular microenvironment. The tool was purposefully built to integrate with current approaches without changes to how the biological experiments were completed over both human-derived cell lines and rodent model systems. Surface coating composition is an important topic in cell culture growth with significant influences on how cells adhere and migrate along the surface. Collagen as a cell coating is frequently used to optimize cell adherence to culture surfaces and guide cells towards distinct phenotypes. An understanding of the composition of collagen coatings for these culture effects are unknown at the spatial and post translational level. The current study profiled that relevant amounts of commercial rat tail collagen that is commonly used for coating of surfaces or preparing thin layers for cultured cells, was compositionally complex. Several types of collagen were found, including collagen α1(XIV) chain, a collagen implicated in enhancing tumor development [72,73]. Specific domains along the collagen structure influence cellular mechanisms, and this finding highlighted new capabilities to define composition and earmark specific domains for further testing in controlling cell culture. Although this approach focused on the visualization and interpretation of collagen composition and distribution as a surface coating, other types of extracellular matrix proteins used in surface coatings should be readily accessible by the combination of enzyme application and scanning approach.

Application demonstrations illustrated the applicability of defining compositional changes in typical biological experiments using cultured cells. A standard 8 chamber well plate was used in these applications. Cells were grown and tested by the collaborative basic research laboratory personnel before handing off the well plate for extracellular analysis. Importantly, cells were seeded at typical low numbers, in this case at 2,500–10,000 cells over cell types of fibroblasts and epithelial cells. Results show that cultured cells secrete compositionally complex collagen types. Collagen compositions were shown to vary by time and were modulated by both drug treatment and genetic knockout. The peptides detected with this method are derived primarily from amino acid protein sequence of triple helical regions and include other conserved domains of collagen structure. Collagen domains have many different types of cellular interactions and exist as a feedback mechanism to the cell microenvironment [74,75]. In time course studies, not all domains showed a linear response, expected if the extracellular microenvironment acts as a feedback mechanism. Certain domains appeared to alter with increases in cell density over time, drug treatment or genetic knockout. Intriguing research has reported that at the coding and noncoding transcription level, collagen types, particularly collagen α1(I) and collagen α2(I) collagen differentially regulate to control processes of proliferation and apoptosis [76,77]. These collective data demonstrated ivECM-MSI as a viable approach to evaluating both cell processes and specific collagen domains. We expect that ivECM-MSI will allow a more detailed view of bioactive domains that work in accordance with cellular status.

The ivECM-MSI approach can readily be adapted for use in many other types of studies. Cell derived extracellular matrix information helps show how cells control their localized extracellular niche and how cells change collagen deposition adapt to the environment. Here visualization by scanning mass spectrometry imaging is an advantage for evaluating the microenvironment secreted by cells. This may be leveraged in co-cultured studies investigating how cell types manipulate the microenvironment in the presence of different cell types. Evaluating the collagen surface during migration and invasion studies may help purposeful design of composition that facilitates specific cell processes across substrates [78,79]. The exploration of 3D cell cultures using ivECM-MSI collagen mass spectrometry imaging may be used to improve in vitro systems that progressively mimic the tissue microenvironment [80,81]. The ability to leverage visual quality control checks on collagen domains during facilitates improved consistency of culture conditions

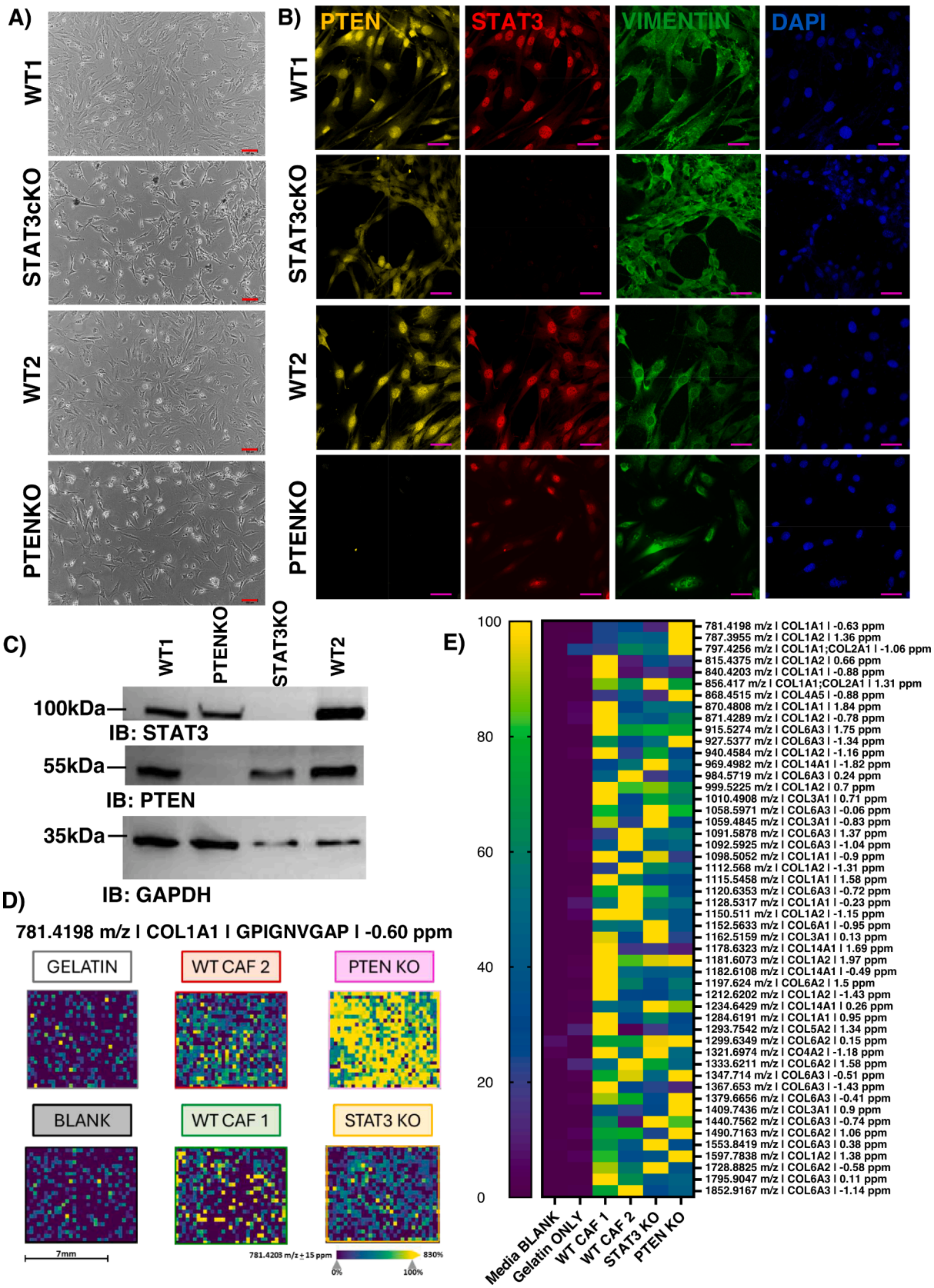

(caption on next page)

Fig. 5. Monitoring the deposition of collagen in mouse primary pancreatic cancer associated fibroblasts on 3 slides using ivECM-MSI and our tissue reference database. A) Phase-contrast microscopy reveals the morphological characteristics of CAFs in culture. These primary fibroblast cells, isolated from mouse pancreatic tissues, exhibit typical spindle-shaped morphology, indicative of their fibroblastic nature. The red scale bar is 100 μm. B) Immunofluorescence staining results depicting the expression patterns of STAT3, PTEN, and the cytoskeletal marker Vimentin in CAFs. Fluorescent signals provide insights into the subcellular localization and relative expression levels of these proteins, contributing to a comprehensive understanding of their roles in CAFs within the context of pancreatic cancer. The magenta scale bar is 50 μm C) Western blot results demonstrating the protein expression levels of STAT3, PTEN, and the housekeeping control GAPDH in CAFs. D) A mass spectrometry imaging heatmap for the peptide relative peak intensities of 1 well per condition/cell line for the putative fibril forming $[M+H]^+$ peptide for collagen α1(I) (GPIGNVGAP) from our tissue reference database. E) Heatmap of the normalized well intensities of 50 features that had putative database matches within 2 ppm mass accuracy. The heatmap includes the following number of samples: a media control with 3 technical replicates (n = wells), a gelatin control with 3 technical replicates (n = wells), fibroblasts from a STAT3 knockout mouse with 2 technical replicates (n = wells) and its wild type parent with 2 technical replicates (WT1; n = wells), and fibroblasts from a PTEN knockout mouse with 4 technical replicates (n = wells) and it's wild type parent with 4 technical replicates (WT2; n = wells). Each feature label includes detected *m/z*, putative protein ID, and parts per million mass deviation from the theoretical $[M+H]^+$ value. Darker blue colors indicate low intensity while brighter yellow colors indicate higher intensities. [HYP] = 1x hydroxylated proline site; (de) = deamidation of asparagine or glutamine; (ox) = methionine oxidation; ppm- parts per million match by mass accuracy. (For interpretation of the references to colour in this figure legend, the reader is referred to the web version of this article.)

due to surface coating, media conditioning and exchange [82].

There is significant need for continued development of technologies that can report ECM composition from cultured cells. Larger cohorts of samples can be easily measured with other commercial MSI instruments reaching 5x the sampling frequency of our scimaX™. While this work focused on scanning by MSI to profile ECM secretion with combined reference libraries, further work enhancing detection around single cell types can improve and understand deposition particularly in mixed-cell experiments. Many of the collagen peptides reported in the current reference lists are isobaric species with variable sites of hydroxylation of proline. The ability to simultaneously track exact sites of hydroxylated proline using ion mobility or tandem MS/MS imaging as a profiling approach would improve targeting capabilities of the technology towards use in evaluating cell quality or cell changes [83,84]. Continued work is being done to develop LC-MS/MS protocols that build out reference libraries with the ability to confirm sequence details of peptides found in cell culture and correlate to those seen in the tissue microenvironment. The current study focused on developing ivECM-MSI using glass as a substrate due to compatibility with instrumentation. The glass slides used in the scanning approach were not conductively coated and are suitable only for charge-decoupled MALDI sources like our instrument. Another option to perform ivECM-MSI on tissue culture plastic would be developing the approach using ionization sources such as desorption electrospray ionization [85,86], nanospray-desorption electrospray ionization [87,88], or the liquid microjunction surface-sampling probe [89,90] mass spectrometry. These electro-spraying ionization sources can be performed in ambient atmosphere and do not require the precise flatness of a glass surface to accurately sample the target. The spectra from MALDI to an electrospray ionization (ESI) source may change due to chemical properties such as hydrophobicity and charge-related parameters of the peptides that influence ionization efficiency [91]. With ESI sources, the MALDI matrix would not be needed, potentially boosting sensitivity and limiting delocalization. Collagen is also not the only component of the extracellular matrix. The extracellular matrix is also composed of elastin, fibronectin, laminins, tenascins, proteoglycans, and other components to name a few [92,93]. A serial application of chondroitinase ABC, PNGaseF, elastase, and collagenase type III to analyze chondroitin sulfate, N-glycans, elastin, and collagen in the same tissue, respectively, was published [94]. With development, the tissue serial enzyme series could be applied to define the in vitro extracellular matrix. Other enzymes may be opportunities to specifically target other components of the extracellular matrix.

To conclude, ivECM-MSI offers a new approach to answer hypotheses directed at understanding in vitro deposition of extracellular matrix in basic biomedical and bioengineering research. Many disease processes are defined by distinctive and predictive collagen stroma regulation that historically have only been defined at the genetic or transcriptomics level or by ambiguous chemical stains. The spatial aspect of this technology may be leveraged against migration assays, co-culture, monitoring transformative processes such as differentiation, and impacts of drug diffusion on ECM secretion. Thus, this proteomic approach provides a way to obtain significant information on the working extracellular microenvironment that is produced and interactive with distinct cell types. Further integration with microscopy modalities and multiplexing targeted enzyme approaches will advance the ability to investigate the complete cellular microenvironment. ivECM-MSI expands capabilities for research to include an understanding of how cells produce and interact with the extracellular microenvironment.

Materials and methods

Rat tail type I collagen coating titrations

Nunc Lab Tek II RS glass 8-chamber slides (Thermo Scientific, 154534) were coated at various concentrations of rat tail collagen type I (EMD Millipore, 08–115). Each well on the 8 chamber slides was coated with a collagen concentration of 0.0 μg/cm^2, 2.5 μg/cm^2, 5.0 μg/cm^2, 10.0 μg/cm^2, 20.0 μg/cm^2, 40.0 μg/cm^2, 80.0 μg/cm^2, or 160.0 μg/cm^2. The collagen stock was diluted to the appropriate concentrations using HPLC grade water (Fisher Scientific, W5-4) so that each well received 200 μL of corresponding solution. After 200 μL of diluted gel solution was dispensed into the corresponding well, the slides were incubated at 37 °C/5% CO_2 for 30 min. After removing and cooling the slides at room temperature, the remaining water was removed by pipette from the slides. The chambers from the slides were removed and remaining water wicked away by a delicate task wipe (Kimberly-Clark, 34120). Slides were then dried in a vacuum desiccator for an hour. Afterwards, the rat tail collagen coated slides were stored in a −20 °C freezer until mass spectrometry imaging preparations.

MDA-MB-231 triple negative breast cancer culture and 7 day titration

Collagen deposition of the poorly differentiated triple negative breast cancer cell line MDA-MB-231 (ATCC, HTB-26) was monitored over a 7-day period. For expansion, stock was thawed in a 37 °C water bath and seeded into a T75 flask with 15 mL of freshly prepared 1x Dulbecco's Modified Eagle Medium (DMEM) with 4.5 g/L glucose, L-glutamine, sodium pyruvate (Corning, 10–0136-CV) with 10 % fetal bovine serum (FBS, Corning, 35–010-CV). The cells were maintained in a humidified incubator at 37 °C with 5 % CO_2 for 5 days and fed daily for expansion. To harvest adhered cells, the media was removed from the flask and 5 mL of Versene (Gibco, 15040066) was added to the flask, incubating at 37 °C for 15 min. Then 2 mL of 1x DMEM with 10 % FBS media was added to the flask and a cell scraper was used to remove any remaining adhered cells from the surface. A portion of the cells were resuspended in a trypan blue solution (Corning, 24-900-COBackspaceI) and counted with a hemacytometer (Hausser Scientific, 1492). After counting, the cells were pelleted at 2000 rpm for 8 min. The supernatant was removed and the cells resuspended to a concentration of 4*10^5

cells/mL in FBS with 10 % dimethyl sulfoxide (DMSO, Fisher Chemical, BP231-100). Aliquots of the cell suspension were dispensed into 7 cryogenic vials (Corning, 430659). Cells were aliquoted in each cryogenic vial to ensure that each well had a 25 μL seed of the cell stock for Lab Tek II 8-chamber slides ($1*10^4$ cells/well). The cryogenic vials were initially frozen in a freezing container (Nalgene, 5100–0001) as per manufacturer's protocol. Aliquots were stored in a liquid nitrogen Dewar until seeding.

To begin monitoring the deposition of collagen over a 7-day experiment, the 1x DMEM with 10 % FBS media and 1 of the 7 aliquoted frozen cell stocks was warmed in a 37 °C water bath. Well #8 in the Lab Tek II 8-chamber slides was filled with 325 μL 1x DMEM with 10 % FBS and seeded with 25 μL of the thawed aliquoted cell stock. Well #1 was filled with 350 μL 1x DMEM with 10 % FBS as a blank control with no cells. The slides were incubated overnight at 37 °C with 5 % CO_2. The next day, 1x DMEM with 10 % FBS and 1 of the remaining 6 aliquoted frozen cell stocks was thawed in a 37 °C water bath. Well #7 in the Lab Tek II 8-chamber slides was filled with 325 μL 1x DMEM with 10 % FBS and seeded with 25 μL of the aliquoted cell stock. The day-old media incubating in the slides were replaced with fresh media. The slides were incubated overnight in at 37 °C with 5 % CO_2. These steps are repeated until the 7th day so that wells #8 through #2 have been seeded incrementally daily and day-old media replaced. Microscope images were acquired a day after the last well (#2) was seeded. Brightfield microscope images were acquired on a AmScope IN200TB Inverted Tissue Culture Microscope using a Samsung Galaxy A52 5G set to 64 megapixels. A 3D printed phone adapter for the microscope was made with PET plastic using files from thingiverse.com (OE-1, OpenOcular). Afterwards, the media was removed from all wells and the slides were placed on ice until mass spectrometry preparation the same day.

H1299 lung carcinoma cell treatment with NS1643 Kv11.1 potassium channel activator

H1299 lung carcinoma cell cycle assay

The H1299 cell line (ATCC; CRL-5803) was cultured in DMEM with 4.5 g/L glucose (Corning, 10-013-CM) supplemented with 10 % FBS (Gemini Bio, 900-208) and 1 % penicillin/streptomycin (Gibco, 15140-122) at 37 °C and 5 % CO_2. Cells were seeded in 6-well plates. After 24 h, cells were treated with DMSO (control) or 50 μM of the Kv11.1 potassium channel activator NS1643 (Alomone Labs, N-115) for 48 h. A cell cycle assay was performed in cells harvested and washed twice with cold PBS. The pellets were resuspended in PBS with 1 % formaldehyde and 0.2 % Triton X-100. Then, the cells were incubated in PBS with DAPI for 2 h. The samples were analyzed with a flow cytometer (LSR Fortessa with HTS, BD Biosciences) and FlowJo (BD Biosciences).

H1299 lung carcinoma cell western blot

Cells were harvested, suspended in PBS (Gibco, 10010–031), and then centrifuged at 3500 rpm for 3 min. The protein pellets were resuspended in 75 μL water and mixed with 25 μL Laemmli sample buffer (Bio-Rad, 1610747) containing β-mercaptoethanol (Thermo Scientific, 125470100). Then, samples were heated at 95 °C for 10 min and centrifuged at 13,000 × g for 5 min. An equal amount of protein were loaded onto SDS-polyacrylamide gel and transferred onto a PVDF membrane. Membranes were blocked with 5 % skimmed milk (RPI, M17200-500) in Tris-Buffered Saline (TBS) (Thermo Scientific, 28358) containing 0.1 % Tween 20 (TBST) for 1 h and then overnight with primary antibodies at 4 °C. All antibodies were purchased from Cell Signaling Technologies, Inc (p21cip1/waf1 Cat# 2947; Histone H3 Cat# 4499). The anti-KCNH2 antibody was purchased from Alomone Lab (APC-016). Membranes were washed three times in TBST and then incubated with a secondary antibody (Cell Signaling Technologies, 7074) for 1 h at room temperature, followed by washing with TBST. Proteins were visualized by the Imager (ChemiDoc MP Imaging System, Bio-Rad). Histone H3 was evaluated for normalization of protein expression.

H1299 lung carcinoma cell senescence β-galactosidase staining kit

H1299 cells were treated with NS1643 for 24hr before staining for β-galactosidase to measure senescence. The Senescence β-Galactosidase Staining Kit was used according to manufacturer's instructions (Cell signaling Technology, Cat. #9860).

H1299 lung carcinoma cell collagen deposition

Two RS glass Lab-Tek II 4-chamber slides (Thermo Scientific, 154526) were seeded with H1299 lung carcinoma cells at $2*10^6$ cells in 3 wells and cultured for 72 h in DMEM supplemented with 10 % FBS and 1 % Penicillin/streptomycin. The fourth chamber only contained media as a blank control with no cells. On day 4, the H1299 cells on one of the slides were treated with 50 μM of NS1643 and the other slide with DMSO for 24 h. On day 5, the media was removed from all wells on both slides. Afterwards, the slides were immediately placed on ice for transport until mass spectrometry preparation the same day.

Human cardiac fibroblast cell culture and spironolactone treatment

Human biopsies were collected in the University hospital at the time of the left ventricular assist device (LVAD) implant and received by the lab. The biopsy was then bisected, and half was used for cell isolation (avg tissue weight for isolation ~ 500 mg). The heart tissue was weighed and then finely minced and incubated with successive changes of collagenase (Liberase Blendzyme 3, Roche No. 05401020001) over two hours with intermittent trituration until digestion was complete. Pooled collagenase fractions were placed in Fibroblast Growth Medium 2 (Promocell, C-23020) with 10 % FBS and 1 % antibiotics/antimycotics to halt collagenase digestion, and then subjected to centrifugation at 1000 rpm for 5 mins at room temperature. Collagenase containing media was removed and cell pellets resuspended in growth media. Cultures were plated at 37 °C. Nonadherent cells were removed ~ 12–18 h after initial plating.

Primary human cardiac fibroblasts untreated and treated with spironolactone were cultured to see the effect of high blood pressure medications on collagen deposition. Primary LVAD human cardiac fibroblasts were seeded at 2,500 cells per well in growth media on Lab Tek II 8-chambered glass slides. Cells were allowed to proliferate for 24 h. Then, 3 wells on each slide were treated with 0.1 mM spironolactone (Sigma-Aldrich, S3378) dissolved in DMSO and 3 wells on each slide were treated with DMSO only. Two wells on each slide contained only media and no cells as a control. Cells were allowed to deposit matrix for 7 days. After deposition, the media was removed from all wells and slides were placed on ice for transport until mass spectrometry preparation the same day.

Mouse pancreatic cancer associated fibroblast cell culture and gene knockout

Pancreatic cancer associated fibroblasts (PCAF) were harvested from pancreatic tissues of KPF model (Pdx1Flpo/+; KrasG12D/+;p53frt/+) [95], KPF Stat3^{cKO} (PdxFlpOki/+; FSF-KrasG12D/+; Trp53frt/frt; FSP-Cre; Stat3fl/fl) [96] and PTEN^{cKO} [97] mice specimens, as previously described [98]. Note in this study that wild-type #1 (WT1) fibroblasts are the parent of the STAT3 knockout mouse. The wild type # 2 (WT2) fibroblasts are the parent of the PTEN knockout cell line. In brief, tumor-bearing pancreas was dissected and minced before being dissociated using the Tumor Dissociation Kit (Miltenyi Biotec, 130-096-730) with a program of 37 m-TDK-1. The resulting digested tissue was then suspended in medium and subjected to gravity-based purification for 10 min. After aspirating the supernatants, the pellets underwent three washes and two additional rounds of gravity sedimentation before being seeded onto tissue culture dishes. This combined approach was used for the isolation of cancer-associated fibroblasts [98]. To ensure complete

STAT3 and PTEN gene knockout from the harvested PCAFs derived from primary culture, a lentiviral-based approach was employed as previously described [96].

Mouse PCAF immunofluorescence staining and confocal microscopy imaging

To assess the protein expression levels of STAT3, PTEN, and Vimentin within PCAFs, immunofluorescence staining was performed. PCAFs were seeded onto sterile 8-well chamber slides (ibidi, 80806) and allowed to adhere. Following fixation in 4 % paraformaldehyde for 15 min, cells were permeabilized with 0.1 % Triton X-100 for 10 min at room temperature. Non-specific binding sites were blocked with 5 % bovine serum albumin (BSA) in PBS for 1 h. Primary antibodies specific to STAT3 (1:100; Cell Signaling, Cat. no. 9139S), PTEN (1:100; Cell Signaling, Cat. no. 9559S), and Vimentin (1:100; R&D SYSTEMS, Cat. no. MAB2105) were then applied to the cells and incubated overnight at 4 °C. After thorough washing with PBS, secondary antibodies conjugated with fluorescent tags (Invitrogen, Alexa Fluor™ 647, Cat. no. A21235; Alexa Fluor™ 594, Cat. no. A32754; & Alexa Fluor™ 488, Cat. no. A21208) were added and incubated for 1 h at room temperature. The mounting medium containing DAPI (4′,6-diamidino-2-phenylindole, Invitrogen, D3571) to stain cell nuclei were added to each well. Zeiss 880 LSM NLO confocal microscope was used to image the fibroblasts. The acquired images were processed using image analysis software (Zeiss, Zen black edition 2.0) to quantify fluorescence intensity and assess protein localization patterns.

Mouse PCAF western blotting

To corroborate the immunofluorescence findings in the mouse pancreatic PCAF and quantify protein expression levels, western blotting was conducted. Total protein was extracted from PCAFs using 1x RIPA buffer (Cell Signaling Technology, 9806) supplemented with phosphatase inhibitors (Sigma, Cat. no. P5726 & P0044:). Protein concentrations were determined using a BCA protein assay kit (Pierce, 23225). Equal amounts of protein were separated by SDS-PAGE and transferred onto PVDF membranes. Membranes were blocked with 5 % non-fat milk in Tris-buffered saline with Tween-20 (TBST) and probed with primary antibodies against STAT3 (1:100; Cell Signaling, Cat. no. 4904S), PTEN (1:100; Cell Signaling, Cat. no. 9559S), and GAPDH (1:100; Cell Signaling, Cat. no. 9559S) overnight at 4 °C. After washing, membranes were incubated with horseradish peroxidase-conjugated secondary antibody Goat Anti-Rabbit IgG (H&L) (Jackson Immunoresearch, 111-035-003) for 1 h at room temperature. Protein bands were visualized using enhanced chemiluminescence reagents (Bio-Rad Laboratories) and quantified using gel documentation iBright software (ThermoFisher). The western blotting analysis provided quantitative data on the expression levels of STAT3 and PTEN in PCAFs, normalized to the GAPDH control.

Mouse PCAF collagen deposition

For the Mouse PCAF collagen deposition monitoring experiment, wells 2 through 8 on the Lab Tek II 8-chamber slides were coated with bovine gel (Sigma, G9136) at a concentration of 0.1 %. Well #1 was not coated with bovine gel as a control. Then, mouse PCAF were seeded in all chambers except #1 and #5 at 2,500 cells per well in 300 µl mL of 1x DMEM, 10 % FBS, 1 % penicillin–streptomycin, and 2 mM L-glutamine media. The blank well #1 and the gel control well #5 were not seeded and were only filled with media. The PCAF were allowed to deposit matrix for 3 days. After deposition, the media was removed from all wells and slides were placed on ice for transport until mass spectrometry preparation the same day.

MALDI mass spectrometry imaging and preparations

Spraying and mass spectrometry protocols were optimized for cell culture collagen deposition based on previous studies in tissue analysis and the workflow has been summarized in Fig. 1 [35,69,94,99–101]. After the cells have been grown on the Lab Tek II 8-chamber slides, media was removed and slides kept on ice for immediate preparation. Slides were decellularized by rinsing each well with one 350 µL aliquot of HPLC grade water. Next, 125 µL of 20 mM ammonium hydroxide (Fisher Chemical, A669S) in water was pipetted in each well and incubated for 5 min [102]. The ammonium hydroxide solution was removed and each well was rinsed with 350 µL of HPLC grade water 4 times to remove any residual debris or base. The slides were air dried for at least 10 min uncovered in the biosafety cabinet. The slides can be stored in a −20 °C freezer if not immediately proceeding to the collagenase digestion. The rat tail collagen coating titration slides did not go through the decellularization process.

A 0.1 mg/mL collagenase III (Worthington, CAT# LSOO4180) solution was made in a 1 mM calcium chloride (Sigma Aldrich, C1016) and 10 mM ammonium bicarbonate (Sigma Aldrich, A6141) buffer. The collagenase solution was then auto sprayed (HTX Technologies, M5) using 7 passes at 40 °C, flow rate of 25 µL/min, nozzle speed of 1200 mm/min, nozzle height of 40 mm, 10 psi nitrogen gas pressure (Airgas, NI UHP300), and with 3 mm track spacing. After collagenase III spraying, the slides were placed in a humidity chamber in a 37 °C oven to incubate for 5 h for digestion of the collagen. After incubation the slides were dried in a vacuum desiccator for 10 min. The slides were stored up to 3 days in a −20 °C freezer if not immediately proceeding to matrix spraying.

After digestion, the MALDI matrix layer was sprayed as a 7 mg/mL α-Cyano-4-hydroxycinnamic acid (CHCA, Millipore, 70990) solution in 1:1 acetonitrile (Fisher Chemical, A998) and HPLC grade water with 0.1 % trifluoroacetic acid (Sigma-Aldrich, T6508). The CHCA matrix solution was then sonicated for 10 min and filtered through a 0.2 µm syringe filter (Millipore, SLLGX13NL) to remove any potential undissolved crystals. (Glu^1)-Fibrinopeptide B human (Sigma-Aldrich, F3261) at 0.106 pmol/µL was added as an internal standard for mass accuracy verification, system suitability evaluation of the instrument, and peak intensity normalization. Matrix was applied by automated sprayer (HTX Technologies, M5) using 4 passes at 79 °C, flow rate of 70 µL/min, nozzle speed of 1300 mm/min, nozzle height of 40 mm, 10 psi nitrogen gas pressure, and with 2.5 mm track spacing. Immediately after spraying the matrix solution, a 5 mM ammonium phosphate (Sigma-Aldrich, 216003) solution was sprayed on top of the matrix on the slides to help reduce matrix cluster formation [103,104]. This was done using 4 passes with 5 mM ammonium phosphate solution over the slides at 60 °C, flow rate of 70 µL/min, nozzle speed of 1300 mm/min, nozzle height of 40 mm, 10 psi of nitrogen gas pressure, and with 3 mm track spacing. The slides were then removed from the sprayer and stored in a vacuum desiccator until mass spectrometry imaging.

Scanning by mass spectrometry imaging was conducted on a Fourier Transform Ion Cyclotron Resonance mass spectrometer (FT-ICR, scimaX™, Bruker Daltonics). Mass spectra were acquired in positive ion mode from a mass range of 630 m/z to 2500 m/z and FID transient of 0.8389 s. The resolving power was measured to be 35,128 at 1570.6768 m/z. The mass spectrometry images were acquired with a laser focus set to small (≈30 µm diameter laser shot), 300 shots per pixel, frequency of 2000 Hz, and raster of 300 µm. This frequency and resolution allowed us to process a slide in the mass spectrometer in less than an hour. Data for mass spectrometry imaging was visualized and extracted using SCiLS Lab 2023c Pro. Putative reference library match identities were made by constructing a script in R Studio 2023.03.1 + 446 to search for feature identities matching a reference database of collagen peptides generated from previous tissue studies [69,99,100] and the LC-MS/MS Reference database we began generating described in the next section. The script to automatically search a reference database by accurate mass is hosted on GitHub in the Angelmslab/CellECMPaper repository (https://github.com/Angelmslab/CellECMPaper). GraphPad Prism 10.0.1 was used to process statistics and visualize the data. Raw mass spectra from MSI were visualized and displayed using mMass version 5.5.0 [105].

LC-MS/MS reference database creation

For de novo LC-MS/MS reference database building, cells were grown on Lab Tek II 8-chamber slides and decellularized as described previously. For each experiment, four wells of an 8-chamber slide were prepared for proteomics. Rat tail collagen experiments were prepared with coating concentrations of 2.5 μg/cm^2 for each well without decellularization. MDA-MB-231 8-chamber slides were grown to confluence for 7 days. PCAF cell line were prepared and grown to confluence as described in the previous section. Afterwards, 300 μL of 7 μg/mL collagenase III solution in 3 mM calcium chloride and 10 mM ammonium bicarbonate buffer was added to each well on the slide. Slides were covered and incubated in a 37 °C oven for 24 h for digestion. After incubation, the peptide solution of each well was desalted using a StageTip (Thermo, SP301) as per manufacturer's protocol. After the StageTip, 4 wells were pooled together for rat tail collagen and MDA-MB-231. Eight wells were pooled together after StageTip for the mouse PCAF cell lines. The pooled samples were dried down via Speed Vac Concentrator (Savant, SVC100H) and reconstituted to extract 2 μg of peptides from solution using a ZipTip (Millipore, ZTC18M096) as per manufacturer's protocol. The 2 μg dried down peptides extracted from the ZipTip were reconstituted in 10 μL of water with 0.1 % formic acid (Fisher Chemical, LS118-4, mobile phase A) for LC-MS/MS analysis. Remaining sample was qualitatively analyzed by pooling all remaining solution from each slide that was left over after the preliminary ZipTip extraction.

LC-MS/MS experiments were performed on a nanoElute high-performance nanoflow liquid chromatography system with trapped ion mobility mass spectrometer (timsTOF flex, Bruker Daltonics). Liquid chromatography separations were performed on a 25 cm × 75 μm ID C18 column (AUR2-25075C18A-CSI, IonOpticks) at a spray voltage of 1600 V and column temperature of 50 °C. Mobile phase A was UHPLC water with 0.1 % formic acid (Fisher Chemical, LS118-4). Mobile phase B was acetonitrile with 0.1 % formic acid (Fisher Chemical, LS120-4). Composition gradient was increased from 2 % to 30 % B from 0 to 40 min and then ramped to 95 % for 7.25 min more until the end at a flow rate of 300 nL/min. Mass spectra were acquired in positive ion mode at a mass range from 100 *m/z* to 1700 *m/z*. MS/MS spectra were acquired in Parallel accumulation–serial fragmentation (PASEF) data dependent acquisition mode. The collisions energies were 20.0 eV at 0.60 1/K_0 and 59.0 eV at 1.60 1/K_0. Th target PASEF mode was 2.0E5 intensity units with a threshold of 2500 intensity units. The number of PASEF ramps was set to 8. The trapped ion mobility spectrometry range for the samples ranged from 0.85 1/K_0 to 1.45 1/K_0. Additional qualitative analysis varied ion mobility range from 0.45 1/K_0 to 1.85 1/K_0. LC-MS/MS data was processed through FragPipe v20.0 [106,107]. Reviewed Swiss-Prot [108] entries from UniProt [109] were used to generate the FASTA sequence database for the FragPipe search downloaded on December 26th, 2023. The UniProt FASTA entries were further filtered using the keyword "extracellular matrix" (KW-0272; GO:0031012) and for the corresponding species for rat (103 entries), human (275 entries), and mouse (247 entries) for the rat tail collagen coatings, MDA-MB-231, and PCAFs LC-MS/MS data, respectively. Variable modifications include proline hydroxylation (P; mass delta 15.9949), asparagine & glutamine deamidation (NQ; mass delta 0.984016), and methionine oxidation (M; mass delta 15.9949). FragPipe search settings included a peptide false discovery rate (FDR) threshold of 0.01, protein FDR threshold of 0.01, and probability threshold of 0.5.

CRediT authorship contribution statement

Stephen C. Zambrzycki: Writing – review & editing, Writing – original draft, Visualization, Validation, Software, Resources, Methodology, Investigation, Funding acquisition, Formal analysis, Data curation, Conceptualization. **Samaneh Saberi:** Writing – review & editing, Visualization, Resources, Methodology, Investigation, Formal analysis. **Rachel Biggs:** Resources, Methodology, Investigation. **Najmeh Eskandari:** Methodology, Investigation. **Davide Delisi:** Investigation. **Harrison Taylor:** Writing – review & editing, Resources, Methodology, Investigation, Conceptualization. **Anand S. Mehta:** Resources, Writing – review & editing. **Richard R. Drake:** Resources, Writing – review & editing. **Saverio Gentile:** Writing – review & editing, Investigation, Formal analysis, Data curation. **Amy D. Bradshaw:** Resources, Methodology, Investigation, Data curation. **Michael Ostrowski:** Methodology, Investigation, Data curation, Conceptualization. **Peggi M. Angel:** Writing – review & editing, Supervision, Project administration, Methodology, Investigation, Funding acquisition, Data curation, Conceptualization.

Declaration of competing interest

The authors declare that they have no known competing financial interests or personal relationships that could have appeared to influence the work reported in this paper.

Data availability

Data will be made available on request.

Acknowledgements

We are grateful for funding support from the Collagen Sequence Variants in Racial Disparities of Breast Cancer grant (NIH/NCI R01 CA253460, PMA), the MUSC Integrative Training in Oncogenic Signaling Fellowship (NIH/NCI T32 CA193201, SZ), the American Cancer Society Postdoctoral Fellowship (PF-23-1029103-01-MM, SZ), and the shared resource grant for the Bruker scimaX™ Magnetic Resonance Mass Spectrometer (NIH/NIGMS S10 OD030212, PMA). Image facilities were supported in part by the Cell & Molecular Imaging Shared Resource, MUSC Cancer Center Support Grant (P30 CA138313), the SC COBRE in Oxidants, Redox Balance, and Stress Signaling (P20 GM103542), the SC COBRE in Digestive and Liver Diseases (P20 GM130457), the MUSC Digestive Disease Research Cores Center (P30 DK123704,) and the Shared Instrumentation Grants S10 OD018113 and S10 OD028663. The cardiac fibroblasts work was partially supported by the Veteran Administration (T32GM132055, RB). The mouse gene knockout pancreatic cancer associated fibroblast work was partially supported by the MUSC Integrative Training in Oncogenic Signaling Fellowship (NIH/NCI T32 CA193201-6, SS) and the Stromal derived IL-6/STAT3 signaling in the development and progression of PDAC (NIH/NCI P01 CA236778-02, MO). We are also grateful for all our collaborators, colleagues, and research communities that provided discussion during this work.

Appendix A. Supplementary data

Supplementary data to this article can be found online at https://doi.org/10.1016/j.mbplus.2024.100161.

References

[1] H. Tomlin, A.M. Piccinini, A complex interplay between the extracellular matrix and the innate immune response to microbial pathogens, Immunology 155 (2) (2018) 186–201.
[2] J. Winkler, A. Abisoye-Ogunniyan, K.J. Metcalf, Z. Werb, Concepts of extracellular matrix remodelling in tumour progression and metastasis, Nature Communications 11 (1) (2020) 5120.
[3] M. Liu, B. López de Juan Abad, K. Cheng, Cardiac fibrosis: myofibroblast-mediated pathological regulation and drug delivery strategies, Adv. Drug Deliv. Rev., 173 (2021) 504–519.
[4] M. Yamauchi, M. Sricholpech, Lysine post-translational modifications of collagen, Essays in Biochemistry 52 (2012) 113–133.
[5] P. Rappu, A.M. Salo, J. Myllyharju, J. Heino, Role of prolyl hydroxylation in the molecular interactions of collagens, Essays in Biochemistry 63 (3) (2019) 325–335.

[6] J.C. Adams, Passing the post: roles of posttranslational modifications in the form and function of extracellular matrix, American Journal of Physiology-Cell Physiology 324 (5) (2023) C1179–C1197.
[7] S. Ricard-Blum, The collagen family, Cold Spring Harbor Perspectives in Biology 3 (1) (2011) a004978–a.
[8] J. Elango, C. Hou, B. Bao, S. Wang, J.E. Maté Sánchez De Val, W. Wenhui, The molecular interaction of collagen with cell receptors for biological function, Polymers, 14(5) (2022) 876.
[9] V.W. Tang, Collagen, stiffness, and adhesion: the evolutionary basis of vertebrate mechanobiology, Molecular Biology of the Cell 31 (17) (2020) 1823–1834.
[10] H. Wang, A review of the effects of collagen treatment in clinical studies, Polymers 13 (22) (2021) 3868.
[11] M. Fang, J. Yuan, C. Peng, Y. Li, Collagen as a double-edged sword in tumor progression, Tumor Biology 35 (4) (2014) 2871–2882. PMID: 24338768.
[12] R. Parenteau-Bareil, R. Gauvin, F. Berthod, Collagen-based biomaterials for tissue engineering applications, Materials 3 (3) (2010) 1863–1887.
[13] S.R. Caliari, J.A. Burdick, A practical guide to hydrogels for cell culture, Nature Methods 13 (5) (2016) 405–414.
[14] C.H. Lee, A. Singla, Y. Lee, Biomedical applications of collagen, International Journal of Pharmaceutics 221 (1–2) (2001) 1–22.
[15] F.H. Silver, G. Pins, Cell growth on collagen: a review of tissue engineering using scaffolds containing extracellular matrix, Journal of Long-Term Effects of Medical Implants 2 (1) (1992) 67–80.
[16] C. Somaiah, A. Kumar, D. Mawrie, A. Sharma, S.D. Patil, J. Bhattacharyya, R. Swaminathan, B.G. Jaganathan, Collagen promotes higher adhesion, survival and proliferation of mesenchymal stem cells, PLoS One1 10 (12) (2015) e0145068.
[17] P. Chua, W.K. Lim, The strategic uses of collagen in adherent cell cultures, Cell Biology International 47 (2) (2023) 367–373.
[18] P. Silva Couto, S.A. Molina, D. O'Sullivan, L. O'Neill, A.M. Lyness, Q.A. Rafiq, Understanding the impact of bioactive coating materials for human mesenchymal stromal cells and implications for manufacturing, Biotechnol. Lett. 45(8) (2023) 1013-1027.
[19] C.G. Fuentes-Corona, J. Licea-Rodriguez, R. Younger, R. Rangel-Rojo, E.O. Potma, I. Rocha-Mendoza, Second harmonic generation signal from type I collagen fibers grown in vitro, Biomed. Opt. Exp. 10 (12) (2019) 6449–6461.
[20] D. Xydias, G. Ziakas, S. Psilodimitrakopoulos, A. Lemonis, E. Bagli, T. Fotsis, A. Gravanis, D.S. Tzeranis, E. Stratakis, Three-dimensional characterization of collagen remodeling in cell-seeded collagen scaffolds via polarization second harmonic generation, Biomed. Opt. Exp. 12 (2) (2021) 1136–1153.
[21] A.M. Barlow, L.B. Mostaço-Guidolin, E.T. Osei, S. Booth, T.-L. Hackett, Super resolution measurement of collagen fibers in biological samples: Validation of a commercial solution for multiphoton microscopy, PLoS One1 15 (2) (2020) e0229278.
[22] A. Stylianou, D. Yova, Surface nanoscale imaging of collagen thin films by atomic force microscopy, Mater. Sci. Eng. C 33 (5) (2013) 2947–2957.
[23] A. Stylianou, Atomic force microscopy for collagen-based nanobiomaterials, J. Nanomater. 2017 (2017) 9234627.
[24] C. Güngörmüş, D. Kolankaya, Characterization of type I, III and V collagens in high-density cultured tenocytes by triple-immunofluorescence technique, Cytotechnology 58 (2008) 145-152.PMC2652553.
[25] O.S. Qureshi, H. Bon, B. Twomey, G. Holdsworth, K. Ford, M. Bergin, L. Huang, M. Muzylak, L.J. Healy, V. Hurdowar, An immunofluorescence assay for extracellular matrix components highlights the role of epithelial cells in producing a stable, fibrillar extracellular matrix, Biology open, 6(10) (2017) 1423–1433. PMC5665462.
[26] A. Harvey, T.-Y. Yen, I. Aizman, C. Tate, C. Case, Proteomic analysis of the extracellular matrix produced by mesenchymal stromal cells: implications for cell therapy mechanism, PLoS One1 8 (11) (2013) e79283.
[27] Y. Taga, M. Kusubata, K. Ogawa-Goto, S. Hattori, Stable isotope-labeled collagen: a novel and versatile tool for quantitative collagen analyses using mass spectrometry, J. Proteome Res. 13 (8) (2014) 3671–3678.
[28] A. Gong, K. Yamada, L. Jing, H. Takeshita, K.-I. Matsumoto, Quantification of Type I Collagen α1 in culture medium using nano-liquid chromatography tandem mass spectrometry, Shimane J. Med. Sci. 38 (1) (2021) 1–5.
[29] C. Hughes, L. Radan, W.Y. Chang, W.L. Stanford, D.H. Betts, L.-M. Postovit, G. A. Lajoie, Mass spectrometry–based proteomic analysis of the matrix microenvironment in pluripotent stem cell culture*, Mol. Cell. Proteom. 11 (12) (2012) 1924–1936.
[30] H. Ragelle, A. Naba, B.L. Larson, F. Zhou, M. Prijić, C.A. Whittaker, A. Del Rosario, R. Langer, R.O. Hynes, D.G. Anderson, Comprehensive proteomic characterization of stem cell-derived extracellular matrices, Biomaterials 128 (2017) 147–159.
[31] A. Naba, K.R. Clauser, S. Hoersch, H. Liu, S.A. Carr, R.O. Hynes, The matrisome: in silico definition and in vivo characterization by proteomics of normal and tumor extracellular matrices, Mol. Cell. Proteom. 11 (4) (2012). M111.014647. PMC3322572.
[32] A. Naba, Ten years of extracellular matrix proteomics: accomplishments, challenges, and future perspectives, Mol. Cell. Proteom. 22 (4) (2023), 100528. PMC10152135.
[33] M. Rafaeva, A.R.D. Jensen, E.R. Horton, K.W. Zornhagen, J.E. Strøbech, L. Fleischhauer, A.E. Mayorca-Guiliani, S.R. Nielsen, D.S. Grønseth, F. Kuś, Fibroblast-derived matrix models desmoplastic properties and forms a prognostic signature in cancer progression, Front. Immunol. 14 (2023), 1154528. PMC10395327.
[34] A.J. Taylor, B.D. Ratner, L.D. Buttery, M.R. Alexander, Revealing cytokine-induced changes in the extracellular matrix with secondary ion mass spectrometry, Acta Biomaterialia 14 (2015) 70–83.
[35] P.M. Angel, S. Comte-Walters, L.E. Ball, K. Talbot, A. Mehta, K.G.M. Brockbank, R.R. Drake, Mapping extracellular matrix proteins in formalin-fixed, paraffin-embedded tissues by MALDI imaging mass spectrometry, J. Proteome Res. 17 (1) (2018) 635–646.
[36] C.L. Clift, S. McLaughlin, M. Munoz, E.J. Suuronen, B.H. Rotstein, A.S. Mehta, R. R. Drake, E.I. Alarcon, P.M. Angel, Evaluation of therapeutic collagen-based biomaterials in the in-farcted mouse heart by extracellular matrix targeted MALDI imaging mass spectrometry, J. Am. Soc. Mass Spectrometry in Press (2021).
[37] M. Kostrzewa, Application of the MALDI Biotyper to clinical microbiology: progress and potential, Expert Rev. Proteom. 15 (3) (2018) 193–202.
[38] T.C. Cain, D.M. Lubman, W.J. Weber Jr, Differentiation of bacteria using protein profiles from matrix-assisted laser desorption/ionization time-of-flight mass spectrometry, Rapid Commun. Mass Spectrometry 8 (12) (1994) 1026–1030.
[39] G. Avila, K. Misch, P. Galindo-Moreno, H.-L. Wang, Implant surface treatment using biomimetic agents, Implant Dentistry 18 (1) (2009) 17–26.
[40] M.J. Landry, F.-G. Rollet, T.E. Kennedy, C.J. Barrett, Layers and multilayers of self-assembled polymers: tunable engineered extracellular matrix coatings for neural cell growth, Langmuir 34 (30) (2018) 8709–8730.
[41] F. Copes, N. Pien, S. Van Vlierberghe, F. Boccafoschi, D. Mantovani, Collagen-based tissue engineering strategies for vascular medicine, Front. Bioeng. Biotechnol. 7 (2019) 166.
[42] M.D. Shoulders, R.T. Raines, Collagen structure and stability, Ann. Rev. Biochem. 78 (2009) 929–958. PMID: 19344236.
[43] K. Yoshida, M. Okada, R. Nagasaka, H. Sasaki, M. Okada, K. Kanie, R. Kato, Time-course colony tracking analysis for evaluating induced pluripotent stem cell culture processes, J. Biosci. Bioeng. 128 (2) (2019) 209–217.
[44] C.M. O'Brien, B.C. Mulukutla, D.G. Mashek, W.-S. Hu, Regulation of metabolic homeostasis in cell culture bioprocesses, Trends Biotechnol. 38 (10) (2020) 1113–1127.
[45] K.V. Kitaeva, C.S. Rutland, A.A. Rizvanov, V.V. Solovyeva, Cell culture based in vitro test systems for anticancer drug screening, Front. Bioeng. Biotechnol. 8 (2020) 322.
[46] M.-H. Yeh, Y.-J. Tzeng, T.-Y. Fu, J.-J. You, H.-T. Chang, L.-P. Ger, K.-W. Tsai, Extracellular matrix–receptor interaction signaling genes associated with inferior breast cancer survival, Anticancer Res. 38 (8) (2018) 4593–4605.
[47] G. Yao, K. Zhao, K. Bao, J. Li, Radiation increases COL1A1, COL3A1, and COL1A2 expression in breast cancer, Open Med. 17 (1) (2022) 329–340.
[48] P. Lin, P. Tian, J. Pang, L. Lai, G. He, Y. Song, Y. Zheng, Clinical significance of COL1A1 and COL1A2 expression levels in hypopharyngeal squamous cell carcinoma, Oncol. Lett. 20 (1) (2020) 803–809.
[49] G. Li, W. Jiang, Y. Kang, X. Yu, C. Zhang, Y. Feng, High expression of collagen 1A2 promotes the proliferation and metastasis of esophageal cancer cells, Ann. Transl. Med. 8 (24) (2020) 1672.
[50] J.L. Chitty, M. Yam, L. Perryman, A.L. Parker, J.N. Skhinas, Y.F.I. Setargew, E.T. Y. Mok, E. Tran, R.D. Grant, S.L. Latham, B.A. Pereira, S.C. Ritchie, K.J. Murphy, M. Trpceski, A.D. Findlay, P. Melenec, E.C. Filipe, A. Nadalini, S. Velayuthar, G. Major, K. Wyllie, M. Papanicolaou, S. Ratnaseelan, P.A. Phillips, G. Sharbeen, J. Youkhana, A. Russo, A. Blackwell, J.F. Hastings, M.C. Lucas, C.R. Chambers, D.A. Reed, J. Stoehr, C. Vennin, R. Pidsley, A. Zaratzian, A.M. Da Silva, M. Tayao, B. Charlton, D. Herrmann, M. Nobis, S.J. Clark, A.V. Biankin, A.L. Johns, D.R. Croucher, A. Nagrial, A.J. Gill, S.M. Grimmond, L.A. Chantrill, A. Chou, T. Dwarte, X.L. Metcalf, G. Jeong, L. Kenyon, N. Waddell, J.V. Pearson, A.-M. Patch, K. Nones, F. Newell, P. Mukhopadhyay, V. Addala, S. Kazakoff, O. Holmes, C. Leonard, S. Wood, O. Hofmann, J.S. Samra, N. Pavlakis, J. Arena, H.A. High, R. Asghari, N.D. Merrett, A. Das, P.H. Cosman, K. Ismail, A. Stoita, D. Williams, A. Spigellman, D. McLeo, J. Kirk, J.G. Kench, P. Grimison, C. Sandroussi, A. Goodwin, R.S. Mead, K. Tucker, L. Andrews, M. Texler, C. Forrest, M. Ballal, D. Fletcher, M. Beilin, K. Feeney, K. Epari, S. Mukhedkar, N. Zeps, N.Q. Nguyen, A.R. Ruszkiewicz, C. Worthley, J. Chen, M.E. Brooke-Smith, V. Papangelis, A.D. Clouston, A.P. Barbour, T.J. O'Rourke, J.W. Fawcett, K. Slater, M. Hatzifotis, P. Hodgkinson, M. Nikfarjam, J.R. Eshleman, R.H. Hruban, C.L. Wolfgang, A. Scarpa, R.T. Lawlor, V. Corbo, C. Bassi, N.B. Jamieson, D.K. Chang, S.B. Dreyer, L. Abdulkhalek, T. Schmitz, V. Lee, K.P. Stewart, M. Arshi, A.M. Steinmann, M. Pajic, P. Timpson, W. Jarolimek, T.R. Cox, I. Australian Pancreatic Cancer Genome, A. Australian Pancreatic Cancer Matrix, A first-in-class pan-lysyl oxidase inhibitor impairs stromal remodeling and enhances gemcitabine response and survival in pancreatic cancer, Nat. Cancer, 4(9) (2023) 1326–1344.
[51] B. Anfuso, C. Tiribelli, L. Adorini, N. Rosso, Obeticholic acid and INT-767 modulate collagen deposition in a NASH in vitro model, Sci. Rep. 10 (1) (2020) 1699.
[52] H.L. Lisa, A.d.A. Joao, D.Z. Joseph, L.P. Maria, A. Carlo, D.N. Steven, S. W. Marlies, L.S. John, K. Klaus-Uwe, C. Ulrich, Pirfenidone safety and adverse event management in idiopathic pulmonary fibrosis, Eur. Respiratory Rev. 26 (146) (2017) 170057.
[53] T. Cai, J. Jiang, W. Yao, Y. Hu, S. Kong, Q. Fan, X. Yan, F. Li, Z. Shi, Pirfenidone inhibits stromal collagen deposition and improves intra-tumoral delivery and antitumor efficacy of Pegylated liposomal doxorubicin, Biomed. Pharmacother. 157 (2023) 114015.
[54] N. Eskandari, V. Senyuk, J. Moore, Z. Kalik, Q. Luan, I. Papautsky, A. Moshiri, M. Bocchetta, S.A. Salami, S. Oryan, S. Gentile, Molecular Activation of the Kv11.1 Channel Reprograms EMT in Colon Cancer by Inhibiting TGFbeta Signaling via Activation of Calcineurin, Cancers (basel) 13 (23) (2021).

[55] V. Senyuk, N. Eskandari, Y. Jiang, R. Garcia-Varela, R. Sundstrom, L. Leanza, R. Peruzzo, M. Burkard, R.D. Minshall, S. Gentile, Compensatory expression of NRF2-dependent antioxidant genes is required to overcome the lethal effects of Kv11.1 activation in breast cancer cells and PDOs, Redox Biol. 45 (2021) 102030.
[56] K. Lansu, S. Gentile, Potassium channel activation inhibits proliferation of breast cancer cells by activating a senescence program, Cell Death Dis. 4 (6) (2013) e652.
[57] C.E. Jones, J.T. Sharick, S.E. Colbert, V.C. Shukla, J.M. Zent, M.C. Ostrowski, S. N. Ghadiali, S.T. Sizemore, J.L. Leight, Pten regulates collagen fibrillogenesis by fibroblasts through SPARC, PLoS One1 16 (2) (2021) e0245653.
[58] W.W. Franke, E. Schmid, M. Osborn, K. Weber, Different intermediate-sized filaments distinguished by immunofluorescence microscopy, Proc. Natl. Acad. Sci. U.S.A. 75 (10) (1978) 5034–5038.
[59] Y. Chen, S. Yang, J. Tavormina, D. Tampe, M. Zeisberg, H. Wang, K. K. Mahadevan, C.-J. Wu, H. Sugimoto, C.-C. Chang, R.R. Jenq, K.M. McAndrews, R. Kalluri, Oncogenic collagen I homotrimers from cancer cells bind to α3β1 integrin and impact tumor microbiome and immunity to promote pancreatic cancer, Cancer Cell 40 (8) (2022) 818–834.e9.
[60] Y. Chen, J. Kim, S. Yang, H. Wang, C.J. Wu, H. Sugimoto, V.S. LeBleu, R. Kalluri, Type I collagen deletion in αSMA(+) myofibroblasts augments immune suppression and accelerates progression of pancreatic cancer, Cancer Cell 39 (4) (2021) 548–565.e6.
[61] P.M. Angel, S. Comte-Walters, L.E. Ball, K. Talbot, K.G.M. Brockbank, A.S. Mehta, R.R. Drake, Mapping Extracellular Matrix Proteins in Formalin-Fixed, Paraffin-embedded Tissues by MALDI Imaging Mass Spectrometry, J. Proteome Res. 17 (1) (2018) 635–646. PMID: 29161047.
[62] P.M. Angel, E. Bruner, C.L. Clift, J.B. Bethard, L.E. Ball, R.R. Drake, C. Feghali-Bostwick, Extracellular Matrix Alterations in Low Grade Lung Adenocarcinoma Compared to Normal Lung Tissue by Imaging Mass Spectrometry, J. Mass Spectrometry 55 (4) (2019) e4450. PMCID: PMC7145762.
[63] P.M. Angel, L. Spruill, M. Jefferson, J.R. Bethard, L.E. Ball, C. Hughes-Halbert, R. R. Drake, Zonal regulation of collagen-type proteins and posttranslational modifications in prostatic benign and cancer tissues by imaging mass spectrometry, The Prostate 80 (2020) 1071–1086. PMCID: PMC7857723.
[64] L.R. Conroy, H.A. Clarke, D.B. Allison, S. Valenca, Q. Sun, T. Hawkinson, L. Young, J. Ferreira, A. Hammonds, J. Dunne, R. McDonald, K. Absher, B. Dong, R. Brunts, K. Markussen, J. Juras, J. Warrent, J. Liu, M. Gentry, P.M. Angel, C. Waters, R.C. Sun, Spatial metabolomics reveals glycogen as an actionable target for pulmonary fibrosis, Nat. Commun. 14 (2023) 2759.
[65] U. Eckhard, E. Schönauer, D. Nüss, H. Brandstetter, Structure of collagenase G reveals a chew-and-digest mechanism of bacterial collagenolysis, Nat. Struct. Mol. Biol. 18 (10) (2011) 1109.
[66] U. Eckhard, P.F. Huesgen, O. Schilling, C.L. Bellac, G.S. Butler, J.H. Cox, A. Dufour, V. Goebeler, R. Kappelhoff, U. auf dem Keller, Active site specificity profiling of the matrix metalloproteinase family: Proteomic identification of 4300 cleavage sites by nine MMPs explored with structural and synthetic peptide cleavage analyses, Matrix Biol. 49 (2016) 37–60. PMC4777984.
[67] C.L. Clift, R.R. Drake, A. Mehta, P.M. Angel, Multiplexed imaging mass spectrometry of the extracellular matrix using serial enzyme digests from formalin-fixed paraffin-embedded tissue sections, Anal. Bioanal. Chem. (2020) 1–11. PMCID: PMC8012227.
[68] C.L. Clift, A.S. Mehta, R.R. Drake, P.M. Angel, Multiplexed imaging mass spectrometry of histological staining, N-glycan and extracellular matrix from one tissue section: a tool for fibrosis research, Methods Mol. Biol. 2350 (2021) 313–329. PMID: 34331294.
[69] D. Rujchanarong, J.E. Lefler, J. Saunders, S. Pippin, L. Spruill, J.B. Bethard, L. E. Ball, A.S. Mehta, R.R. Drake, M.C. Ostrowski, P.M. Angel, Defining the tumor microenvironment by integration of immunohistochemistry and extracellular matrix targeted imaging mass spectrometry, Cancers 13 (17) (2021) 4419. PMCID: PMC8430776.
[70] J. Dunne, J. Griner, M. Romeo, J. Macdonald, C. Krieg, M. Lim, G. Yagnik, K. J. Rothschild, R.R. Drake, A.S. Mehta, P.M. Angel, Evaluation of antibody-based single cell imaging techniques coupled to multiplexed imaging of N-glycans and collagen peptides by matrix-assisted laser desorption/ionization mass spectrometry imaging, analytical bioanaytical, Chemistry 415 (28) (2023) 7011–7024. PMCID: PMC10632234.
[71] M. Hu, Z. Ling, X. Ren, Extracellular matrix dynamics: tracking in biological systems and their implications, J. Biol. Eng. 16 (1) (2022) 1–13.
[72] J. Winkler, A. Abisoye-Ogunniyan, K.J. Metcalf, Z. Werb, Concepts of extracellular matrix remodelling in tumour progression and metastasis, Nat. Commun. 11 (1) (2020) 1–19.
[73] M.W. Pickup, J.K. Mouw, V.M. Weaver, The extracellular matrix modulates the hallmarks of cancer, EMBO Rep. 15 (12) (2014) 1243–1253.
[74] S.M. Sweeney, J.P. Orgel, A. Fertala, J.D. McAuliffe, K.R. Turner, G.A. Di Lullo, S. Chen, O. Antipova, S. Perumal, L. Ala-Kokko, Candidate cell and matrix interaction domains on the collagen fibril, the predominant protein of vertebrates, J. Biol. Chem. 283 (30) (2008) 21187–21197. PMCID: PMC2475701.
[75] M. Assunção, D. Dehghan-Baniani, C.H.K. Yiu, T. Später, S. Beyer, A. Blocki, Cell-derived extracellular matrix for tissue engineering and regenerative medicine, Front. Bioeng. Biotechnolo. 8 (2020) 602009.
[76] J. Li, Y. Gao, Q. Li, L. Chen, Y. Chen, J. Li, LncRNA COL1A2-AS1 promotes skin fibroblast apoptosis by repressing p-Smad3 and promoting β-catenin expression, Experiment. Dermatol. 30 (8) (2021) 1090–1098.
[77] L. Tang, Y. Liang, H. Xie, X. Yang, G. Zheng, Long non-coding RNAs in cutaneous biology and proliferative skin diseases: advances and perspectives, Cell Proliferation 53 (1) (2020) e12698.
[78] N. Kramer, A. Walzl, C. Unger, M. Rosner, G. Krupitza, M. Hengstschläger, H. Dolznig, In vitro cell migration and invasion assays, Mutation Res./Rev. Mutation Res. 752 (1) (2013) 10–24.
[79] J. Pijuan, C. Barceló, D.F. Moreno, O. Maiques, P. Sisó, R.M. Marti, A. Macià, A. Panosa, In vitro cell migration, invasion, and adhesion assays: from cell imaging to data analysis, Front Cell Dev. Biol. 7 (2019) 107.
[80] K.M. Yamada, E. Cukierman, Modeling tissue morphogenesis and cancer in 3D, Cell 130 (4) (2007) 601–610.
[81] J. Franco-Barraza, D.A. Beacham, M.D. Amatangelo, E. Cukierman, Preparation of extracellular matrices produced by cultured and primary fibroblasts, Curr. Protocols Cell Biol. 71 (2016) 10.9.1–10.9.34.
[82] R.R. Lareu, I. Arsianti, H.K. Subramhanya, P. Yanxian, M. Raghunath, In vitro enhancement of collagen matrix formation and crosslinking for applications in tissue engineering: a preliminary study, Tissue Eng. 13 (2) (2007) 385–391.
[83] J. Stauber, L. MacAleese, J. Franck, E. Claude, M. Snel, B.K. Kaletas, I.M.V. D. Wiel, M. Wisztorski, I. Fournier, R.M.A. Heeren, On-tissue protein identification and imaging by MALDI-ion mobility mass spectrometry, J. Am. Soc. Mass Spectrometry 21 (3) (2010) 338–347.
[84] B.M. Prentice, C.W. Chumbley, R.M. Caprioli, High-speed MALDI MS/MS imaging mass spectrometry using continuous raster sampling, J. Mass Spectrometry 50 (4) (2015) 703–710.
[85] M.W. Towers, T. Karancsi, E.A. Jones, S.D. Pringle, E. Claude, Optimised Desorption Electrospray Ionisation Mass Spectrometry Imaging (DESI-MSI) for the Analysis of Proteins/Peptides Directly from Tissue Sections on a Travelling Wave Ion Mobility Q-ToF, J. Am. Soc. Mass Spectrometry 29 (12) (2018) 2456–2466.
[86] T. Soudah, A. Zoabi, K. Margulis, Desorption electrospray ionization mass spectrometry imaging in discovery and development of novel therapies, Mass Spectrometry Rev. 42 (2) (2023) 751–778.
[87] O.J. Hale, H.J. Cooper, Native mass spectrometry imaging of proteins and protein complexes by nano-DESI, Anal. Chem. 93 (10) (2021) 4619–4627.
[88] M. Yang, D. Unsihuay, H. Hu, F. Nguele Meke, Z. Qu, Z.Y. Zhang, J. Laskin, Nano-DESI mass spectrometry imaging of proteoforms in biological tissues with high spatial resolution, Anal. Chem. 95 (12) (2023) 5214–5222.
[89] V. Kertesz, M. Khalid, S.T. Retterer, J.F. Cahill, Structure-driven liquid microjunction surface-sampling probe mass spectrometry, Anal. Chem. (2023).
[90] J.F. Cahill, M. Khalid, S.T. Retterer, C.L. Walton, V. Kertesz, In situ chemical monitoring and imaging of contents within microfluidic devices having a porous membrane wall using liquid microjunction surface sampling probe mass spectrometry, J. Am. Soc. Mass Spectrometry 31 (4) (2020) 832–839.
[91] W.M. Nadler, D. Waidelich, A. Kerner, S. Hanke, R. Berg, A. Trumpp, C. Rösli, MALDI versus ESI: the impact of the ion source on peptide identification, J. Proteome Res. 16 (3) (2017) 1207–1215.
[92] J.K. Kular, S. Basu, R.I. Sharma, The extracellular matrix: Structure, composition, age-related differences, tools for analysis and applications for tissue engineering, J. Tissue Eng. 5 (2014), 2041731414557112.
[93] L. Schaefer, R.M. Schaefer, Proteoglycans: from structural compounds to signaling molecules, Cell Tissue Res. 339 (1) (2010) 237–246.
[94] C.L. Clift, R.R. Drake, A. Mehta, P.M. Angel, Multiplexed imaging mass spectrometry of the extracellular matrix using serial enzyme digests from formalin-fixed paraffin-embedded tissue sections, Anal. Bioanal. Chem. 413 (10) (2021) 2709–2719.
[95] J. Wu, X. Liu, S.G. Nayak, J.R. Pitarresi, M.C. Cuitiño, L. Yu, B.E. Hildreth 3rd, K. A. Thies, D.J. Schilling, S.A. Fernandez, G. Leone, M.C. Ostrowski, Generation of a pancreatic cancer model using a Pdx1-Flp recombinase knock-in allele, PLoS One1 12 (9) (2017) e0184984.
[96] J.E. Lefler, C.B. MarElia-Bennett, K.A. Thies, B.E. Hildreth 3rd, S.M. Sharma, J. R. Pitarresi, L. Han, C. Everett, C. Koivisto, M.C. Cuitino, C.D. Timmers, E. O'Quinn, M. Parrish, M.J. Romeo, A.J. Linke, G.A. Hobbs, G. Leone, D. C. Guttridge, T.A. Zimmers, G.B. Lesinski, M.C. Ostrowski, STAT3 in tumor fibroblasts promotes an immunosuppressive microenvironment in pancreatic cancer, Life Sci Alliance 5 (11) (2022).
[97] J.R. Pitarresi, X. Liu, A. Avendano, K.A. Thies, G.M. Sizemore, A.M. Hammer, B. E. Hildreth 3rd, D.J. Wang, S.A. Steck, S. Donohue, M.C. Cuitiño, R.D. Kladney, T. A. Mace, J.J. Chang, C.S. Ennis, H. Li, R.H. Reeves, S. Blackshaw, J. Zhang, L. Yu, S.A. Fernandez, W.L. Frankel, M. Bloomston, T.J. Rosol, G.B. Lesinski, S. F. Konieczny, D.C. Guttridge, A.K. Rustgi, G. Leone, J.W. Song, J. Wu, M. C. Ostrowski, Disruption of stromal hedgehog signaling initiates RNF5-mediated proteasomal degradation of PTEN and accelerates pancreatic tumor growth, Life Sci. Alliance 1 (5) (2018) e201800190.
[98] X. Liu, J.R. Pitarresi, M.C. Cuitiño, R.D. Kladney, S.A. Woelke, G.M. Sizemore, S. G. Nayak, O. Egriboz, P.G. Schweickert, L. Yu, S. Trela, D.J. Schilling, S. K. Halloran, M. Li, S. Dutta, S.A. Fernandez, T.J. Rosol, G.B. Lesinski, R. Shakya, T. Ludwig, S.F. Konieczny, G. Leone, J. Wu, M.C. Ostrowski, Genetic ablation of Smoothened in pancreatic fibroblasts increases acinar-ductal metaplasia, Genes Dev. 30 (17) (2016) 1943–1955.
[99] C.L. Clift, S. McLaughlin, M. Muñoz, E.J. Suuronen, B.H. Rotstein, A.S. Mehta, R. R. Drake, E.I. Alarcon, P.M. Angel, Evaluation of therapeutic collagen-based biomaterials in the infarcted mouse heart by extracellular matrix targeted MALDI imaging mass spectrometry, J. Am. Soc. Mass Spectrometry 32 (12) (2021) 2746–2754.
[100] P.M. Angel, L. Spruill, M. Jefferson, J.R. Bethard, L.E. Ball, C. Hughes-Halbert, R. R. Drake, Zonal regulation of collagen-type proteins and posttranslational modifications in prostatic benign and cancer tissues by imaging mass spectrometry, The Prostate 80 (13) (2020) 1071–1086.

[101] P.M. Angel, E. Bruner, J. Bethard, C.L. Clift, L. Ball, R.R. Drake, C. Feghali-Bostwick, Extracellular matrix alterations in low-grade lung adenocarcinoma compared with normal lung tissue by imaging mass spectrometry, J. Mass Spectrometry 55 (4) (2020) e4450.
[102] A.L. Hellewell, S. Rosini, J.C. Adams, A Rapid, Scalable method for the isolation, functional study, and analysis of cell-derived extracellular matrix, J. Visualized Experiments (119) (2017).
[103] I.P. Smirnov, X. Zhu, T. Taylor, Y. Huang, P. Ross, I.A. Papayanopoulos, S. A. Martin, D.J. Pappin, Suppression of α-cyano-4-hydroxycinnamic acid matrix clusters and reduction of chemical noise in MALDI-TOF mass spectrometry, Anal. Chem. 76 (10) (2004) 2958–2965. PMID: 15144210.
[104] Y. Ucal, A. Ozpinar, Improved spectra for MALDI MSI of peptides using ammonium phosphate monobasic in MALDI matrix, J. Mass Spectrometry 53 (8) (2018) 635–648.
[105] M. Strohalm, M. Hassman, B. Košata, M. Kodíček, mMass data miner: an open source alternative for mass spectrometric data analysis, Rapid Commun. Mass Spectrometry 22 (6) (2008) 905–908.
[106] A.T. Kong, F.V. Leprevost, D.M. Avtonomov, D. Mellacheruvu, A.I. Nesvizhskii, MSFragger: ultrafast and comprehensive peptide identification in mass spectrometry–based proteomics, Nat. Methods 14 (5) (2017) 513–520.
[107] G.C. Teo, D.A. Polasky, F. Yu, A.I. Nesvizhskii, Fast deisotoping algorithm and its implementation in the MSFragger search engine, J. Proteome Res. 20 (1) (2021) 498–505.
[108] E. Gasteiger, E. Jung, A. Bairoch, SWISS-PROT: connecting biomolecular knowledge via a protein database, Curr. Issues Mol. Biol. 3 (3) (2001) 47–55.
[109] T.U. Consortium, UniProt: the Universal Protein Knowledgebase in 2023, Nucl. Acids Res. 51 (D1) (2022) D523–D531.